



Active Faulting in Lake Constance (Austria, Germany, Switzerland) Unraveled by Multi-Vintage Reflection Seismic Data

S.C. Fabbri^{1*}, C. Affentranger¹, S. Krastel², K. Lindhorst², M. Wessels³, Herfried Madritsch⁴, R. Allenbach⁵, M. Herwegh¹, S. Heuberger⁶, U. Wielandt-Schuster⁷, H. Pomella⁸, T. Schwestermann⁸ and F.S. Anselmetti¹

¹Institute of Geological Sciences and Oeschger Centre of Climate Change Research, University of Bern, Bern, Switzerland, ²Institute of Geosciences, Christian-Albrechts-Universität zu Kiel, Kiel, Germany, ³Institut für Seenforschung der LUBW, Langenargen, Germany, ⁴National Cooperative for the Disposal of Radioactive Waste (NAGRA), Wettingen, Switzerland, ⁵Federal Office of Topography Swisstopo, Wabern, Switzerland, ⁶Department of Earth Sciences, ETH Zürich, Zürich, Switzerland, ⁷Landesamt für Geologie, Rohstoffe und Bergbau Baden-Württemberg, Freiburg i. Br., Germany, ⁸Department of Geology, University of Innsbruck, Innsbruck, Austria

OPEN ACCESS

Edited by:

Francesco Emanuele Maesano,
Istituto Nazionale di Geofisica e
Vulcanologia (INGV), Italy

Reviewed by:

Chiara Amadori,
University of Pavia, Italy
Alessandro Maria Michetti,
University of Insubria, Italy

*Correspondence:

S.C. Fabbri
stefano.fabbri@geo.unibe.ch

Specialty section:

This article was submitted to
Structural Geology and Tectonics,
a section of the journal
Frontiers in Earth Science

Received: 21 February 2021

Accepted: 23 July 2021

Published: 11 August 2021

Citation:

Fabbri SC, Affentranger C, Krastel S, Lindhorst K, Wessels M, Madritsch H, Allenbach R, Herwegh M, Heuberger S, Wielandt-Schuster U, Pomella H, Schwestermann T and Anselmetti FS (2021) Active Faulting in Lake Constance (Austria, Germany, Switzerland) Unraveled by Multi-Vintage Reflection Seismic Data. *Front. Earth Sci.* 9:670532. doi: 10.3389/feart.2021.670532

Probabilistic seismic hazard assessments are primarily based on instrumentally recorded and historically documented earthquakes. For the northern part of the European Alpine Arc, slow crustal deformation results in low earthquake recurrence rates and brings up the necessity to extend our perspective beyond the existing earthquake catalog. The overdeepened basin of Lake Constance (Austria, Germany, and Switzerland), located within the North-Alpine Molasse Basin, is investigated as an ideal (neo-) tectonic archive. The lake is surrounded by major tectonic structures and constrained via the North Alpine Front in the South, the Jura fold-and-thrust belt in the West, and the Hegau-Lake Constance Graben System in the North. Several fault zones reach Lake Constance such as the St. Gallen Fault Zone, a reactivated basement-rooted normal fault, active during several phases from the Permo-Carboniferous to the Mesozoic. To extend the catalog of potentially active fault zones, we compiled an extensive 445 km of multi-channel reflection seismic data in 2017, complementing a moderate-size GI-airgun survey from 2016. The two datasets reveal the complete overdeepened Quaternary trough and its sedimentary infill and the upper part of the Miocene Molasse bedrock. They additionally complement existing seismic vintage data that investigated the mass-transport deposit chronology and Mesozoic fault structures. The compilation of 2D seismic data allowed investigating the seismic stratigraphy of the Quaternary infill and its underlying bedrock of Lake Constance, shaped by multiple glaciations. The 2D seismic sections revealed 154 fault indications in the Obersee Basin and 39 fault indications in the Untersee Basin. Their interpretative linkage results in 23 and five major fault planes, respectively. One of the major fault planes, traceable to Cenozoic bedrock, is associated with a prominent offset of the lake bottom on the multibeam bathymetric map. Across this area, high-resolution single channel data was acquired and a transect of five short cores was retrieved displaying significant sediment thickness changes across the seismically mapped fault trace with a surface-rupture related turbidite, all indicating repeated activity of a likely seismogenic

strike-slip fault with a normal faulting component. We interpret this fault as northward continuation of the St. Gallen Fault Zone, previously described onshore on 3D seismic data.

Keywords: coring, earthquakes, seismic hazard, seismic stratigraphy, active faults, glacial overdeepening, turbidites, Molasse basin

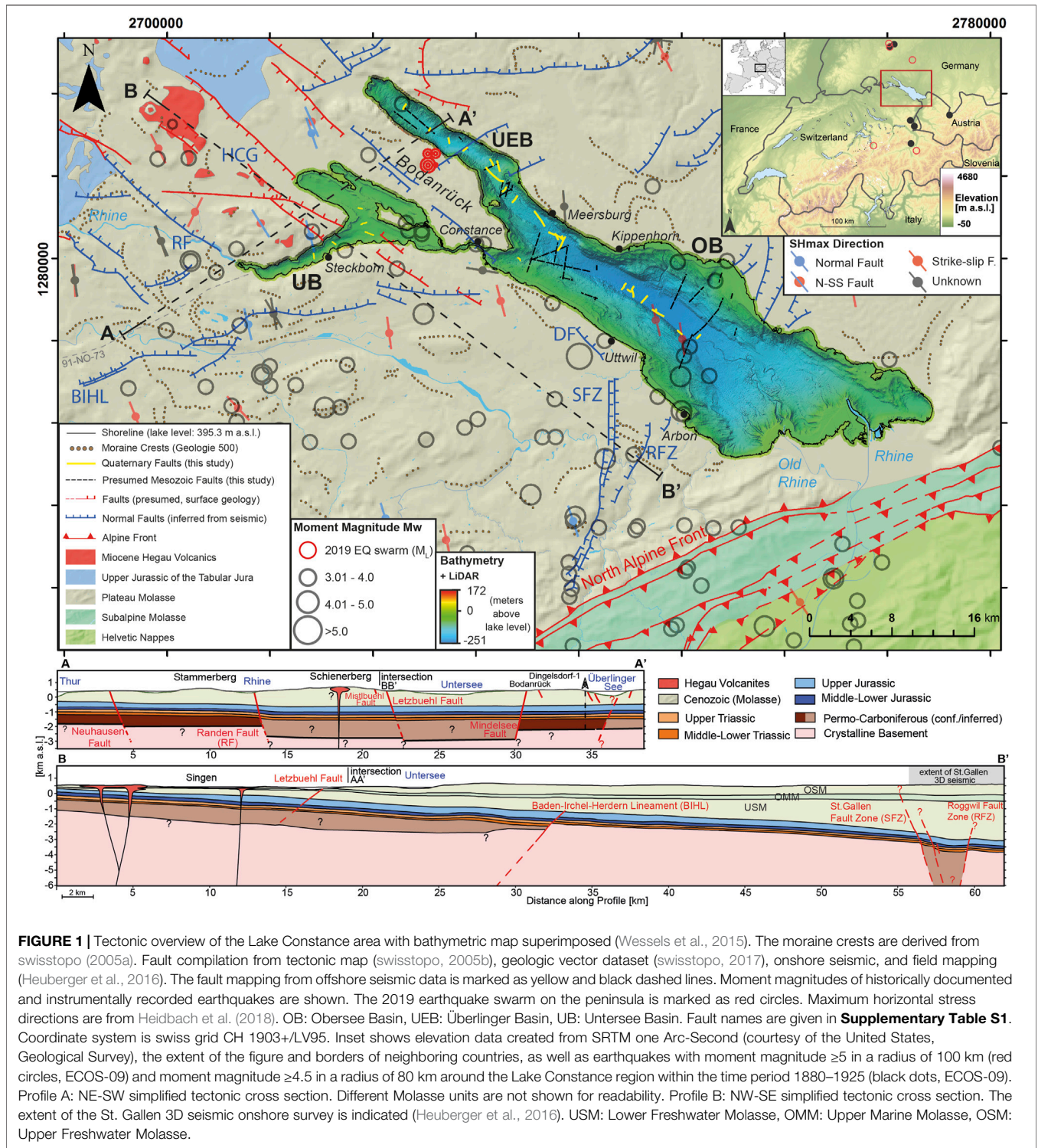
INTRODUCTION

In intraplate environments with low crustal deformation rates such as in the North Alpine Front area (e.g., Houlié et al., 2018), current probabilistic seismic hazard assessments are primarily based on historically documented and instrumentally recorded earthquakes (Wiemer et al., 2009), especially since documentation of active faults is sparse. The earthquake catalogue of Switzerland (e.g., Fäh et al., 2011) builds such a basis for hazard assessment, covering a time span of roughly 1,000 years with ~20,000 events. The limited temporal coverage of instrumentally recorded and historically reported events motivates the approach to use primary and secondary paleoseismic evidence, known as on- and off-fault records, respectively, and to expand the time span of the existing database. Such “paleoseismic” data aim at documenting prehistoric earthquakes throughout the Holocene and Late Pleistocene, reflecting recent tectonic activity and characterizing location, timing, and size of events (McCalpin and Nelson, 2009).

In recent years, large efforts have been made to overcome the limited time span of historically documented and instrumentally recorded earthquakes in the Alps by the investigation of secondary evidence such as earthquake-triggered subaquatic mass movements and their related turbidites (Becker et al., 2002; Schnellmann et al., 2002; Monecke et al., 2004; Kremer et al., 2015b; Sammartini et al., 2021) and small-scale *in situ* deformation features (e.g., liquefaction structures, micro-faults, mushroom-like intrusions) in lake sediments (Rodriguez-Pascua et al., 2000; Monecke et al., 2004; Schnellmann et al., 2006). Despite this convincing off-fault evidence suggesting several strong earthquakes and several distinct phases of increased activity between 300–600, 1,400–1700, 2,200–2,500, 3,000–3,600, 6,200–7,000 and at around 9,500–9,900 calibrated years before present in the Alpine realm, there is a general absence of known seismogenic fault structures with clear surface ruptures supporting these observations (Kremer et al., 2020). Their identification is absolutely vital though to minimize uncertainties associated with the calculated recurrence time of strong earthquakes. In recent years, paleoseismological research has provided a wealth of information about paleoseismicity (Michetti et al., 2005), but is often related to the successful identification of specific events on recognized active faults (Strasser et al., 2013). To this date, indications for Quaternary tectonic deformations in the Alpine foreland are subtle and distinct traces of significant Quaternary movements, such as offset post-glacial features or topographic displacements, are rare (Wiemer et al., 2009; Madritsch et al., 2010; Strasser et al., 2013). Only few successful identifications of primary

evidence in active fault systems within Switzerland have been reported (Ustaszewski et al., 2007; Kremer et al., 2020), such as the identified active normal fault near the eastern edge of the Upper Rhine Graben, identified by geomorphological and geophysical analysis, supplemented by six trenches at two different sites (Meghraoui, 2001), or the roughly 4 km long strike-slip fault crossing the shoreline of Lake Thun (Fabbri et al., 2017). This is mostly due to three factors, 1) high erosion rates in the Alpine region and strong landscape modifications by glacio-fluvial processes in the Alpine foreland, 2) pervasive anthropogenic landscape modification (Ustaszewski et al., 2007) and 3) a minimum threshold of moment magnitude that needs to be exceeded in order to create surface rupture (Wells and Coppersmith, 1994; Stirling et al., 2002). The first two factors can be addressed by focusing on almost erosion free environments, such as perialpine lakes. The latter factor requires imaging the subsurface spatially densely to various depths, so that the investigated time span is expanded to several thousand years. This guarantees the required vertical and lateral resolution, increasing the likelihood of discovering the roots of high-magnitude events offsetting lacustrine sediments. However, the confirmation of on-fault evidence is often solely possible via a multidisciplinary approach combining information from geophysical (e.g., seismic, electromagnetic, radar data), geomorphological (bathymetric, lidar, satellite imagery) and geological (outcrop, core, geochemical analysis) independent datasets (Fabbri et al., 2017; Oswald et al., 2021). Hence, only few study sites in lacustrine settings showed on-fault paleoseismic evidence documenting active faulting in the Alpine realm, such as Lake Garda (South of the Alps in northern Italy) with mass-movement deposits and seismo-turbidites close to interpreted active tectonic deformations (Gasparini et al., 2020), Lake Le Bourget (northwestern French Alps) with Riedel-like expressions of Quaternary deformation in the Holocene sediments related to onshore strike-slip faults (de La Taille et al., 2015), or inner-alpine Lake Achensee (eastern Austrian Alps) with offset postglacial sediment infill unraveled by multiple, coeval mass wasting deposits (Oswald et al., 2021). The predominantly accumulative character and high preservation potential of Lake Constance (Austria, Germany, and Switzerland, inset **Figure 1**) may serve as an ideal laboratory to unravel existing fault structures and lake-bottom offsets.

In Lake Constance, we conducted a high-resolution multi-channel seismic pilot-survey with a moderate-sized airgun in 2016 that revealed the complete Quaternary overdeepened trough and its sedimentary infill and the upper part of the Molasse bedrock, including a bedrock-rooting and Holocene sediment-offsetting fault structure. This motivated us to conduct a new seismic survey on Lake Constance to image



the deeper subsurface of the perialpine lake to greater detail and depth by complementing and densifying the existing grids with a slightly modified setup. The airgun survey was carried out to build a database that enables us to 1) seismically image the deep subsurface to the Cenozoic strata below the lake, 2) document the morphology and the infilling stratigraphy of the Quaternary

trough shaped by multiple glaciations, 3) map shallow fault structures, observed in Quaternary deposits, but likely rooting in stratigraphically deeper bedrock and correlate them to offshore fault systems and 4) identify recently (Holocene) active faults and characterize them with high resolution single channel seismic data and short core transects.

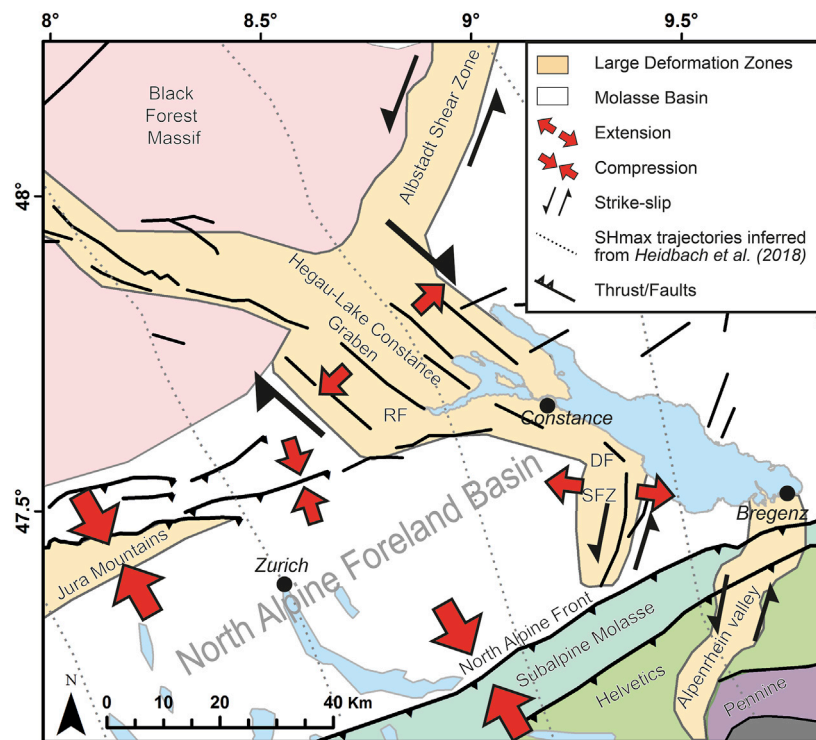


FIGURE 2 | Simplified kinematic model for a selection of large-scale deformation zones in the North Alpine Foreland Basin (modified after Egli et al., 2016 and Ring and Gerdes, 2016). Estimated maximum horizontal stress (SHmax) trajectories are inferred from Heidbach et al. (2018). DF: Dozwil Fault, RF: Randen Fault, SFZ: St. Gallen Fault Zone (also see **Supplementary Table S1**).

Geological Setting, Present Stress Field and Seismicity

The sedimentary subsurface of trinational Lake Constance has been studied intensively (e.g., Müller and Gees, 1968; Niessen et al., 1990; Wessels, 1998; Wessels et al., 2010). Lake Constance was a typical oligotrophic, perialpine lake until the beginning of the 20th century, when it turned eutrophic (Wessels et al., 1999; Hanisch et al., 2009). Most of the detrital material is delivered by its primary inflow the Alpine River Rhine (Wessels, 1998). The glacially overdeepened Lake Constance (Preusser et al., 2010) covers an area of ~540 km² with a total volume of ~50 km³ and a maximum water depth of 251.1 m relative to a longterm reference level of 395.3 m a.s.l. at Constance (Wessels et al., 2015). The lake is divided into Lower Lake Constance (Untersee Basin, UB) and Upper Lake Constance which is further separated in Obersee (OB) and Ueberlingen Basin (UEB, **Figure 1**).

Major tectonic structures surround Lake Constance: the North Alpine Front in the South (Zerlauth et al., 2014; Ortner et al., 2015; Pomella et al., 2015), bordering the detached Subalpine Molasse, the Jura fold-and-thrust belt in the West and the Hegau-Lake Constance Graben System (HCG) to the North (Roth et al., 2010; Ibele, 2015; Malz et al., 2016, **Figure 2**). The Alpine Front is interrupted by the NNE trending Alpenrhein valley, which shows a sinistral transtension along the valley (Ring and Gerdes, 2016). The system is conjugated with a dextral transtension along the WNW striking HCG system (Ring and Gerdes, 2016). The lake

basin itself is part of the North Alpine Foreland Basin (NAFB, **Figure 2**) that was formed by flexural bending of the European lithosphere due to crustal thickening in the Alps in Cenozoic times (Allen et al., 1986) and slab rollback, driven by the gravitational pull of the European slab (Schlunegger and Kissling, 2015).

The Cenozoic deposits of the Molasse Basin encompass four lithostratigraphic units: Lower Marine Molasse, Lower Freshwater Molasse, followed by the Upper Marine Molasse and the Upper Freshwater Molasse (Pffiffer, 1986; Schreiner, 1992). The Molasse units rest unconformably on the primarily marine, SSE dipping Mesozoic sedimentary sequence represented by Jurassic to Triassic formations (Heuberger et al., 2016). The Mesozoic strata rest on either the crystalline basement or on the Permo-Carboniferous infill of Paleozoic troughs. The former is expected to be structurally complex as witnessed in the Black Forest in southern Germany where it consists of pre-Variscan amphibolite-grade gneisses and migmatites, Variscan and post-Variscan plutonic intrusions that are dissected by Permo-Carboniferous half grabens also reported to the west of the lake (Egli et al., 2016; Madritsch et al., 2018).

The NAFB hosts many fault structures surrounding the Lake Constance area, derived from surface geology, and inferred from on- and offshore seismic data (**Figure 1**). A compilation of the most important fault zones (Roth et al., 2010; Sommaruga et al., 2012; Egli et al., 2016; Heuberger et al., 2016) within the NAFB, including their kinematics, offset and shallowest displaced units,

is given in **Supplementary Table S1**. The St. Gallen Fault Zone (SFZ), closely investigated by 3D seismic survey (Heuberger et al., 2016), is a NNE-SSW striking set of normal faults in the NAFB with multiphase tectonic activity. The basement-rooted normal faults of the SFZ are ideally oriented in the current stress field of NNW-SSE oriented maximum horizontal stress (SHmax) to be presently reactivated in sinistral strike-slip fashion (Heuberger et al., 2016). The northern end of the SFZ tends to bend anticlockwise towards a N-S strike and terminates in front of the southwestern shoreline of the OB. The SFZ is surrounded by several other normal faults, such as the Roggwil Fault Zone (RFZ) or the Dozwil Fault (DF) with a vertical offset of up to 270 m in the Mesozoic strata, reaching into the Upper Freshwater Molasse. The Randen Fault (RF) belongs to the roughly NW-SE striking Hegau-Lake Constance Graben System (Ibele, 2015, Egli et al., 2016). Northwest of the lake, its trace is constrained by surface outcrops and 2D seismic imaging. Immediately NW of the Untersee, the RF is well defined. Two branches are inferred with the NW-SE striking branch close to the UB showing a combined NE-down vertical offset of 225 m (Hofmann et al., 2000; Egli et al., 2016). Further to the east, the Mindelsee Fault is a parallel-striking fault roughly following the Bodanrück ridge that separates the UB from the UEB (**Figure 1**). Finally, the Baden-Irchel-Herdern Lineament (BIHL, e.g., Naef et al., 1995) represents a ENE-WSW striking normal fault zone. It is associated with the southern boundary of the Permo-Carboniferous trough of northern Switzerland (Malz et al., 2016; Madritsch et al., 2018) and inferred to run just south of the UB presumably crossing the OB. Offshore fault structures derived from airgun seismic data, acquired between December 1980 and February 1981 (Prakla Seismos GmbH, 1982), cross the lake in deeper units (Cenozoic and Mesozoic), striking predominantly NNE-SSW in OB and NW-SE in the West of UEB. These fault orientations are particularly prone to reactivation when taking the recent tectonic stress field into account. Northeast of Lake Constance, SHmax is N-S oriented, and rotates gradually anticlockwise along the Alpine Front from East to West by $\sim 40^\circ$ (Heidbach and Reinecker, 2013; Heidbach et al., 2018), as inferred from various data sources as earthquake focal mechanisms, geophysical logs and geological data.

The Lake Constance area is impacted by several historical and instrumentally recorded seismic events, most recently by a swarm of earthquakes north of the city of Constance at the southwestern shoreline of UEB (red dots, **Figure 1**) and an earthquake northwest of UB associated to the HCG (February 05, 2021, local magnitude 3.2, ~ 11 km depth, swiss seismological service). The swarm included at least 30 events, with local magnitudes registering up to 3.7 (M_L , July 30, 2019) and hypocenters shallower than 5 km depth on the peninsula are evidence of ongoing seismic activity in the region (Diehl et al., 2020). The strongest historically known earthquake occurred in 1771 CE with a moment magnitude of $M_W = 5.1$. Its epicenter was located close to the Dozwil Fault (DF), just a few kilometers away from the southwestern shoreline of OB. Within a radius of less than 100 km from Lake Constance (Uttwil: 47.58373° N, 9.34119° E), five major earthquakes with $M_W \geq 5.4$ are historically documented (ECOS-09, Fäh et al., 2011). The most recent

three of them (1911, 1935, 1943 CE) occurred in southern Germany between 50 and 80 km away from Uttwil with M_W between 5.4 and 5.6 (**Figure 1**).

METHODS

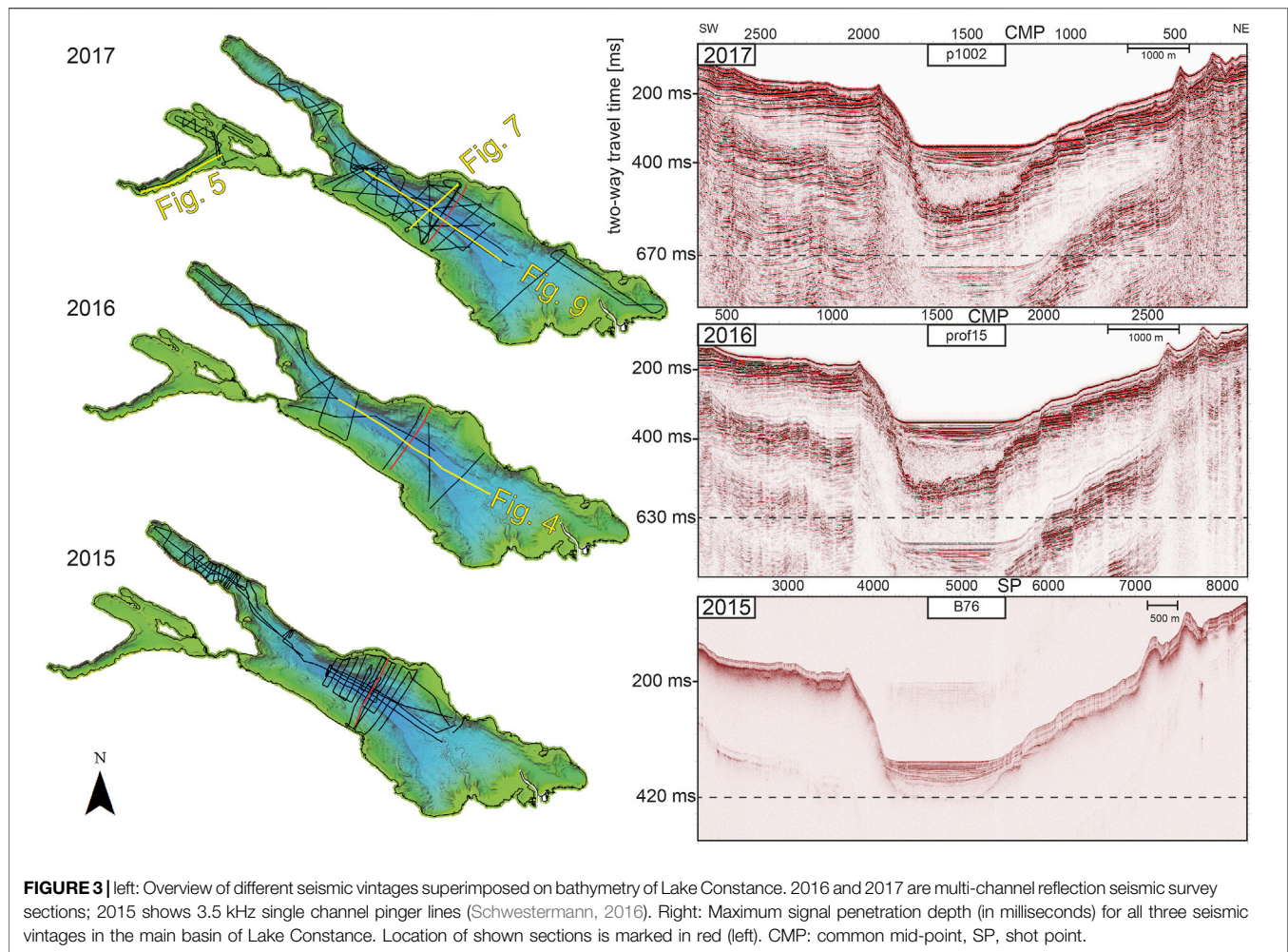
Seismic Surveys

First reflection seismic data were acquired in the years 1980 and 1981 by a collaboration of various industry partners (Prakla Seismos GmbH, 1982). These data were analyzed in the framework of the project ACoRE-B (2010–2013; alpS GmbH Innsbruck).

The main basis of the investigation reported here is formed by a series of new seismic data sets acquired between 2015 and 2019. An overview of these datasets is provided in **Supplementary Table S2** including information on sources, source volume, shot interval, vertical (Widess, 1973; Chopra et al., 2006) and horizontal resolution, channel distance, total recorded length and the targeted basins. 488 km of multi-channel reflection seismic data was acquired in 2016 and 2017. The Mini GI Gun survey from 2016 was a pilot study dedicated to the OB and UEB (Lemke, 2006), targeting Molasse bedrock and the lake's sedimentary infill with a total recorded length of 43.2 km (**Figure 3**). Due to the success of the survey, a densified grid of seismic sections was shot using a slightly larger GI Gun 210 for the OB (353 km). The smaller source from 2016 was applied in the UB (92 km). The shallow water and narrow bays justified the smaller gun and a shorter streamer to ensure maneuvering capabilities. Generally, the larger GI gun allows for a deeper penetration at the cost of reduced lateral and vertical resolution. Since the GI gun requires more air at a constant buffer bottle pressure compared to the Mini GI Gun, the limited air output of the compressor requires an increase in shot interval and shot spacing (maintaining same cruising speed 7.5–10 km/h) from ~ 6 –8 m (Mini GI) to ~ 20 –22.5 m (GI Gun), what impacts data resolution and penetration depth significantly. **Figure 1** illustrates the effective impact of using different seismic vintages by comparing the reached depth in two-way travel times (twt) for the same section across the OB. The depth penetration gain from using a three times larger GI air gun instead of a Mini GI gun are relatively small. The penetration increases from 630 to 670 ms twt (depth is always reported as twt, if not mentioned otherwise) at the price of reduced resolution (vertical: 2.5 vs 1.9 m; lateral: 23.7 vs 20.5 m, respectively). A typical GI Gun line in OB (e.g., Line p201) shows a fold between seven and eight for more than 80% of the data with a bin width of 3 m. More than 70% of the data shows a fold between 8 and 11 for a typical line in UB (e.g., Line p601) with a bin width of 2 m.

In addition, high-resolution single-channel pinger seismic data were acquired between 2015 and 2019 (**Supplementary Table S2**). These were processed using a 1800–2000–6,000–6,500 Hz bandpass (BP) filter (Schwestermann, 2016) and a BP filter of 1800–2,200–6,000–6,500 Hz, respectively. Simple GPS receivers with precision to a few meters (e.g., Garmin GPS 72H, for 2019) were used to measure the line navigation.

The processing steps for the 2016 multi-channel air gun data involved conversion from SEG-D to SEG-Y data format, bulk shifting (-10 ms), debias, spherical divergence correction, BP



filtering (10–20–1,000–1,500 Hz), geometry correction (shot point), normal-move-out (NMO) correction (1,500 m/s), common-midpoint (CMP) stacking (bin size = 3 m), second BP filtering (60–120–600–1,200 Hz), and migration at a constant velocity (1,500 m/s). VISTA has been used as processing software. Navigation was measured using a Trimble GPS receiver.


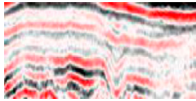
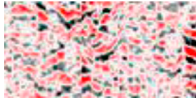
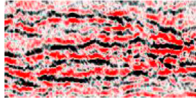
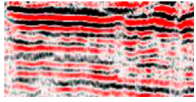
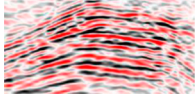
The processing of the multi-channel air gun data from 2017 involved setting up the geometry, binning, first-break picking of linear move-out for trace shifting, debias, automated gain control, BP filtering (25–35–700–850 Hz), NMO analysis and internal velocity analysis from nearby onshore boreholes (Swisspetrol, 1962) used for velocity model creation and stacking, surface-related multiple elimination, Eigenvector filtering, FX-Deconvolution, post-stack 2D time migration using finite differences. PROMAX has been used as processing software. For quality control during the survey, debias, bulkshift (19 ms), geometry creation, binning, noise removal, simple velocity model with two picks, predictive deconvolution, stacking and finite difference migration have been applied to the raw data. VISTA has been used as processing software for onsite quality control. Navigation was measured with a Leica GX 1230 GNSS with a precision of ~1.5 m.

Multibeam Bathymetry Data and Coring

In 2013, a multibeam bathymetric campaign on Lake Constance revealed the detailed morphology of the lake bottom **Figure 1** and **Figure 2**, (Wessels et al., 2015). The bathymetric map with a resolution of 3 m was acquired within the project “Tiefenschärfe” (Wessels et al., 2015), which aimed at a seamless terrain model of the entire lake bottom surface (OB, UEB and UB) combining laser scanning for water depths shallower than 5 m and multibeam echo sounder images for all deeper zones. The bathymetric survey was conducted using a Kongsberg EM 2040 Multibeam echo sounder (1° × 1° beam width, 300 kHz standard operating frequency) on the Research Vessel “Kormoran” (Wessels et al., 2015).

Based on the findings of the various seismic surveys, a short coring campaign was designed and conducted in September 2019 using the “Kormoran”. A transect of five short cores with up to 2 m length was taken in the deepest part of Lake Constance, across a morphological step that was detected by various seismic vintages and bathymetric data. The cores were opened, stratigraphically described and line-scanned using a Geotek Multi-Sensor Core Logger. A Garmin GPS 72H was used for navigation purposes.

TABLE 1 | Overview of seismic facies, expected lithology and interpretation.

| Facies ID | Seismic facies | Description | Expected lithology |
|-----------|---|--|---|
| SF6 |  | Parallel, high-amplitude continuous horizontal reflections, with semi-transparent intercalated sections | Lacustrine sedimentation (sand to clay) with intercalated turbidites; increasing <i>in-situ</i> sediment production |
| SF5 |  | Transparent to semi-transparent chaotic facies at the base with faint internal stratification, medium amplitudes towards the top | Mostly sand and glacial mud, with coarse material at the base; transition from proximal (till) to more distal fine-grained glacio-lacustrine deposition |
| SF4 |  | Transparent to semi-transparent chaotic facies | Diamict, glacial mud with dropstones, coarse gravelly base; till with shore-parallel eskers on the flanks |
| SF3 |  | Semi-transparent chaotic facies at top, medium-amplitude reflections at the base | Transition Molasse –Till; oldest glacial sediments |
| SF2 |  | Medium-amplitude, laterally continuous reflections | Molasse—Bedrock; characterized by strong over-deepening and several bedrock troughs |
| SF1 |  | Low-amplitude continuous reflections | Limestone - Mesozoic |

RESULTS

Seismic Facies and Horizons

The overall seismic stratigraphy of Lake Constance shows six seismic stratigraphic units (U1—U6) characterized by six different seismic facies (SF1—SF6, **Table 1**). Drilling information to geologically characterize these seismic facies is very limited. Recently, a new drilling technique with an advanced piston coring tool was tested in Lake Constance reaching a subsurface depth of 24 m (Harms et al., 2020), expanding significantly previous coring limits (maximum core depth of 8.7 m; Wessels, 1998; Hanisch et al., 2009; Schwab et al., 2013). Nevertheless, this drill core only calibrates the uppermost seismic unit (U6). Since lithological and sedimentological information from cores is lacking for the deeper sections, the stratigraphic and lithologic interpretations are mainly based on seismic facies analysis and seismic stratigraphy.

Accordingly, the overall stratigraphy of the lake's subsurface shows from bottom to top a succession of Mesozoic and Cenozoic bedrock (U1 and U2), a transitioning bedrock-till layer (U3), glacial till (U4), glacio-lacustrine (U5) and lacustrine deposits (U6, **Figure 4**). This general stratigraphy can be further subdivided into additional seismic subunits within the glacial tills (e.g., **Figure 4**, U4b), glacio-lacustrine and lacustrine deposits based on characteristic seismic facies changes, unconformities and prominent strong reflections that are beyond the scope of this study. All stratigraphic sequences are clearly discernable in the central basin of the lake, where seismic reflections are laterally continuous and bedrock morphology shows significant overdeepening with steep flanks rising to the NE and SW. Recognition of single sequences is more difficult and partially

impeded towards the coastlines, where the top of bedrock shallows and where gas-rich delta deposits of the Rhine River Delta blank the data.

Mesozoic (U1) Strata and Cenozoic (U2) Bedrock

The seismic facies of the Mesozoic (U1), only identified in the UB, shows low-amplitude continuous reflections (SF1, **Table 1**) at the top, and rather transparent to semi-transparent chaotic facies (SF4) in the core of the unit. Two different reflection intervals (I and II) can be distinguished (**Figure 5**), with the top of the first interval showing low-amplitude reflections between 500 and 700 ms, and a second package with undulating topography between 0.8 and 1.2 s. These apparently do not match overlying reflections and are therefore interpreted as of primary and not multiple origin. Nonetheless, the uncertainty of the depth of the Mesozoic remains large. In those areas where the Mesozoic was identified, the broad depth-range of the formation is remarkable (**Figure 6**). In the OB, despite a larger air gun being used, signal penetration is not strong enough to image the Mesozoic strata. An interpreted onshore NE-SW seismic reflection profile from Nagra **Figure 1** (Naef et al., 1995), is in direct prolongation of the Untersee and shows good agreement with the depth of the Base Molasse at ~600 ms depth (Top Mesozoic reflection interval I) and Top Lias at ~1 s (Top Mesozoic reflection interval II).

The Cenozoic bedrock (U2) consists of Miocene Molasse deposits. In the OB, its seismic facies is characterized by laterally continuous medium-amplitude parallel reflections (SF2) at the top and generally dipping southeastward towards the Alps. The top of U2 is marked by an erosional unconformity. The recognition of U2 is only hampered in areas of presumably gas-rich Quaternary sediments where multiples prevail. In the

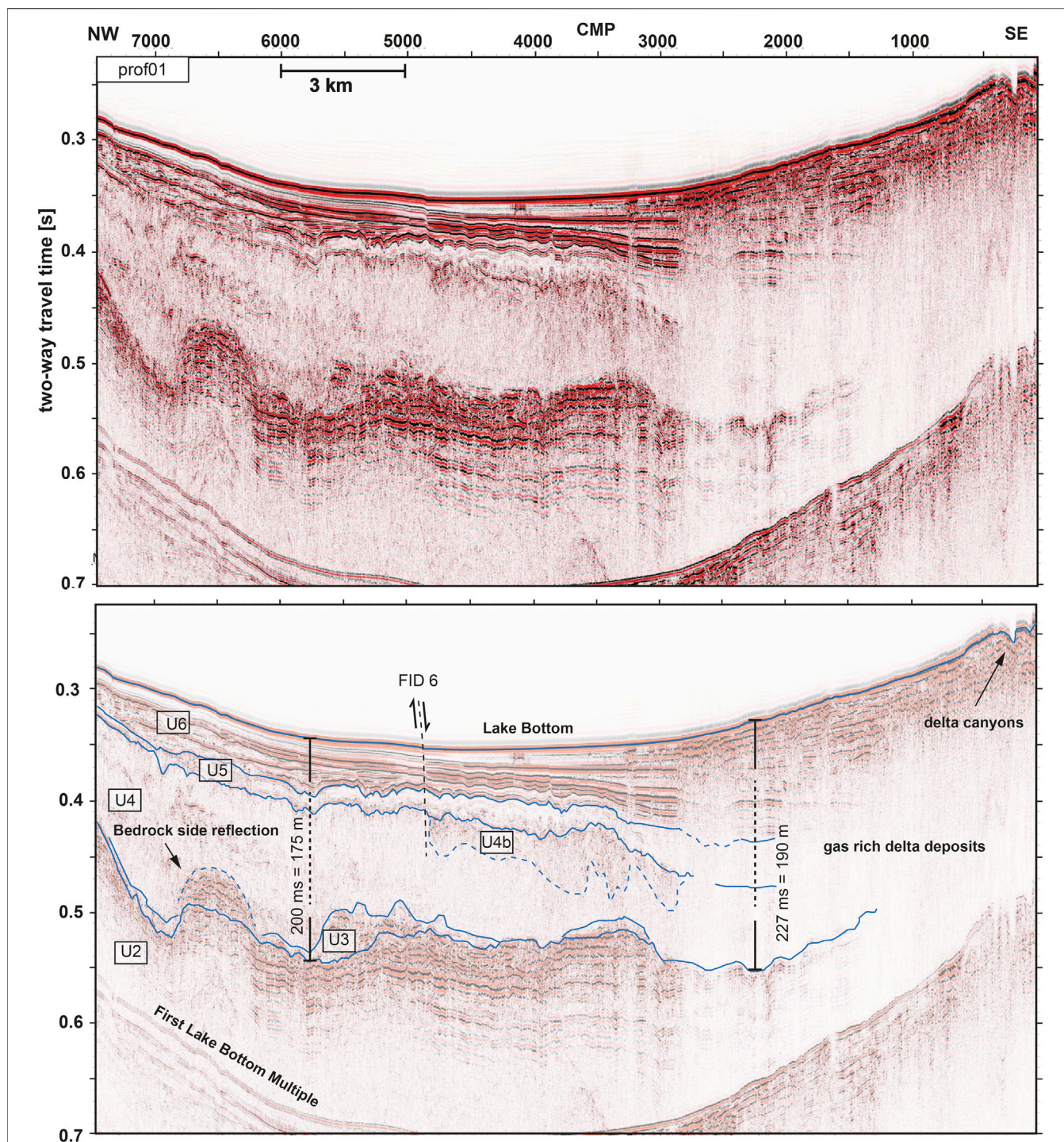
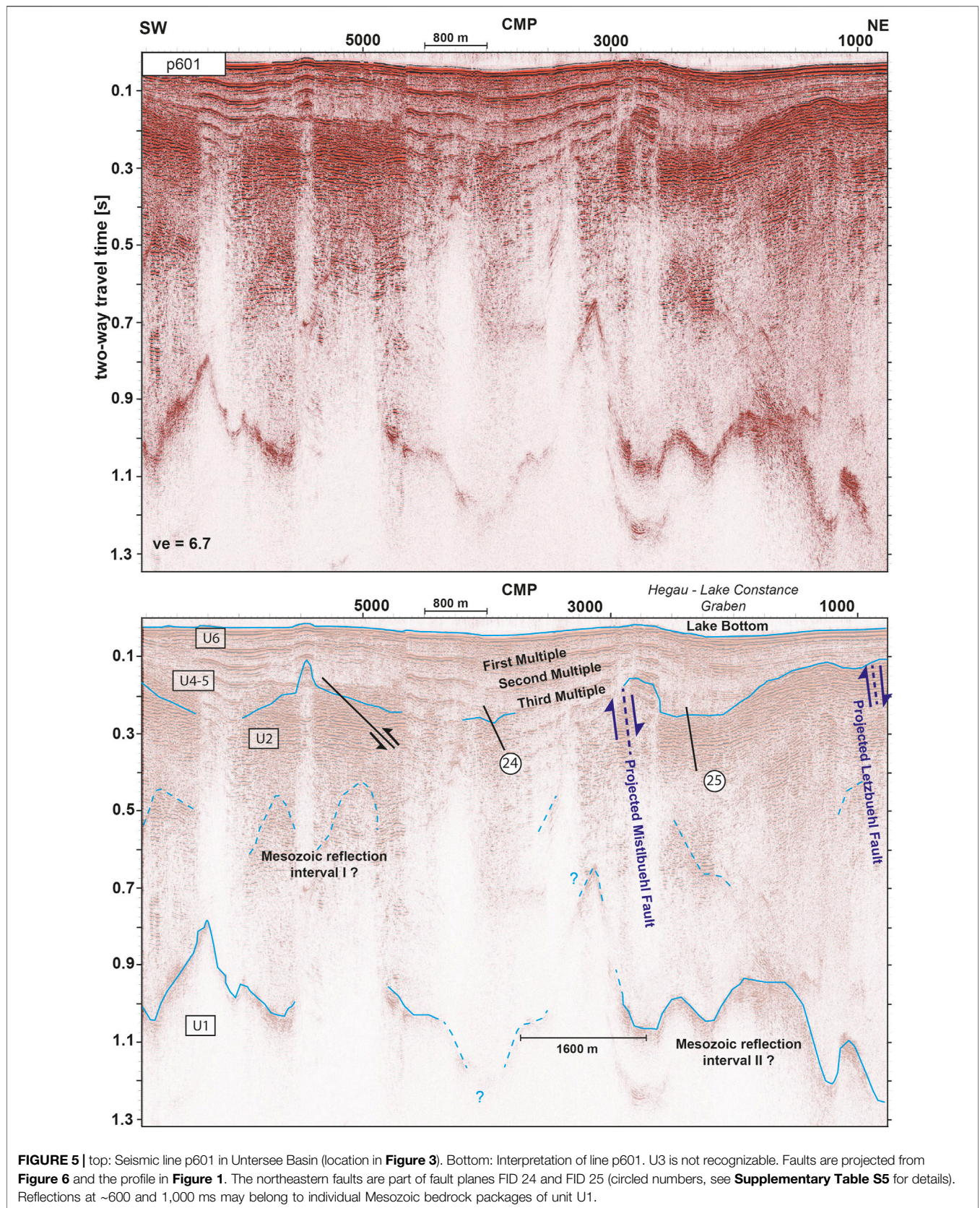
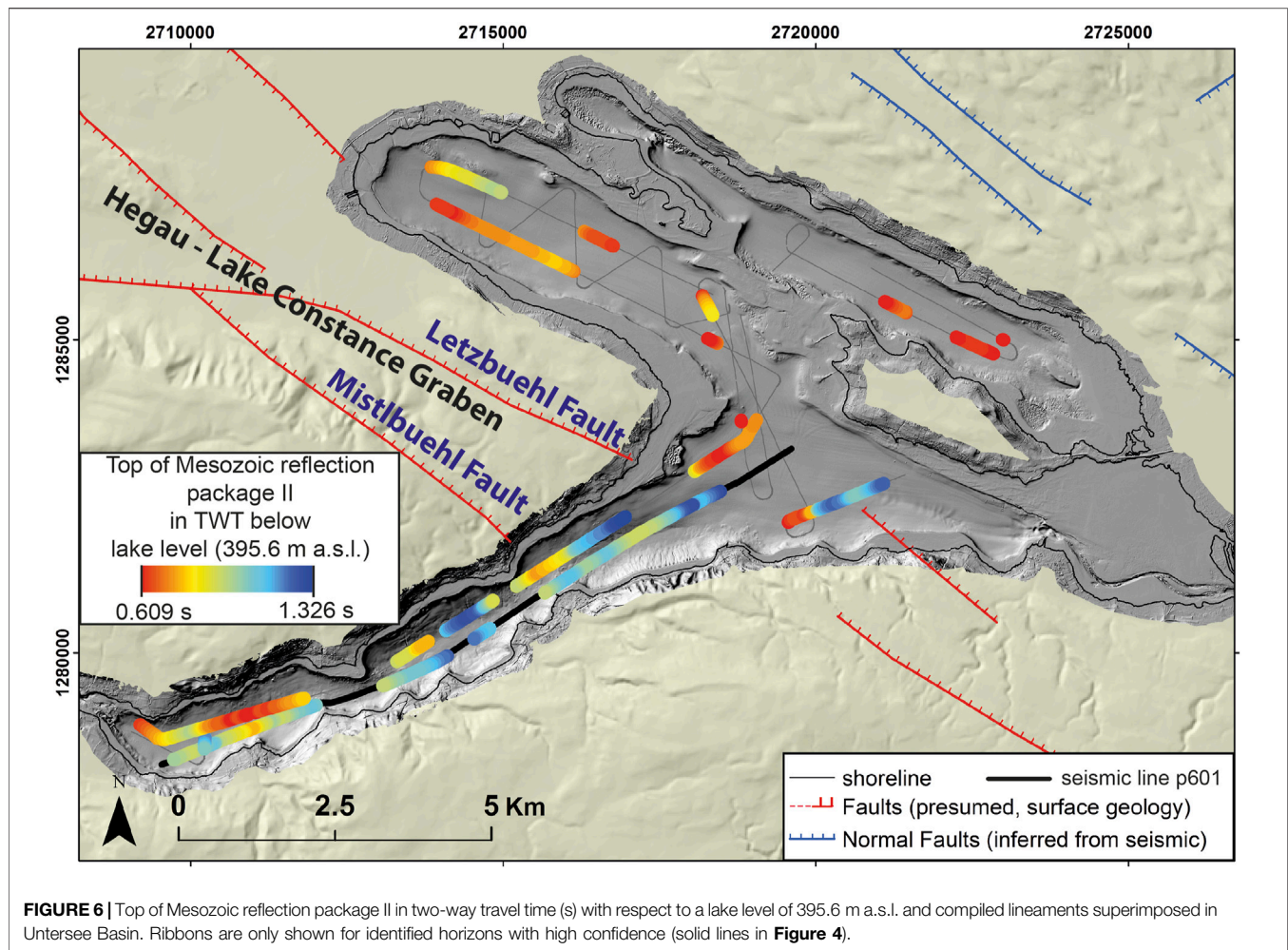


FIGURE 4 | top: Multi-channel reflection seismic data of line prof01 along the OB (location in **Figure 3**). Bottom: Interpretation of seismic section with five stratigraphic units U2-U6 (compare **Table 1**). Further subdivision of the main units (e.g., U4b) mark prominent disturbances of the main units. Offset reflections in unit U6 at CMP 5000 culminate at the lake bottom and show normal faulting. Gas-rich delta deposits prohibit signal penetration in the SE. 190 m and 175 m sediment coverage can be observed in the delta distal area and the central basin, respectively, taking interval velocities into account (**Supplementary Table S3**). Note that bedding of Molasse bedrock U2 is clearly visible, and allows investigating bedrock-rooting active fault structures (FID 6—Kippenhorn Fault).

UB, the shallow water amplified the challenge of bedrock recognition due to the occurrence of strong lake-bottom multiples.

Our seismic data confirms a major bedrock trough is developed underneath Lake Constance previously described by Müller and Gees (1968) and (Finckh et al., 1984). In the OB, the





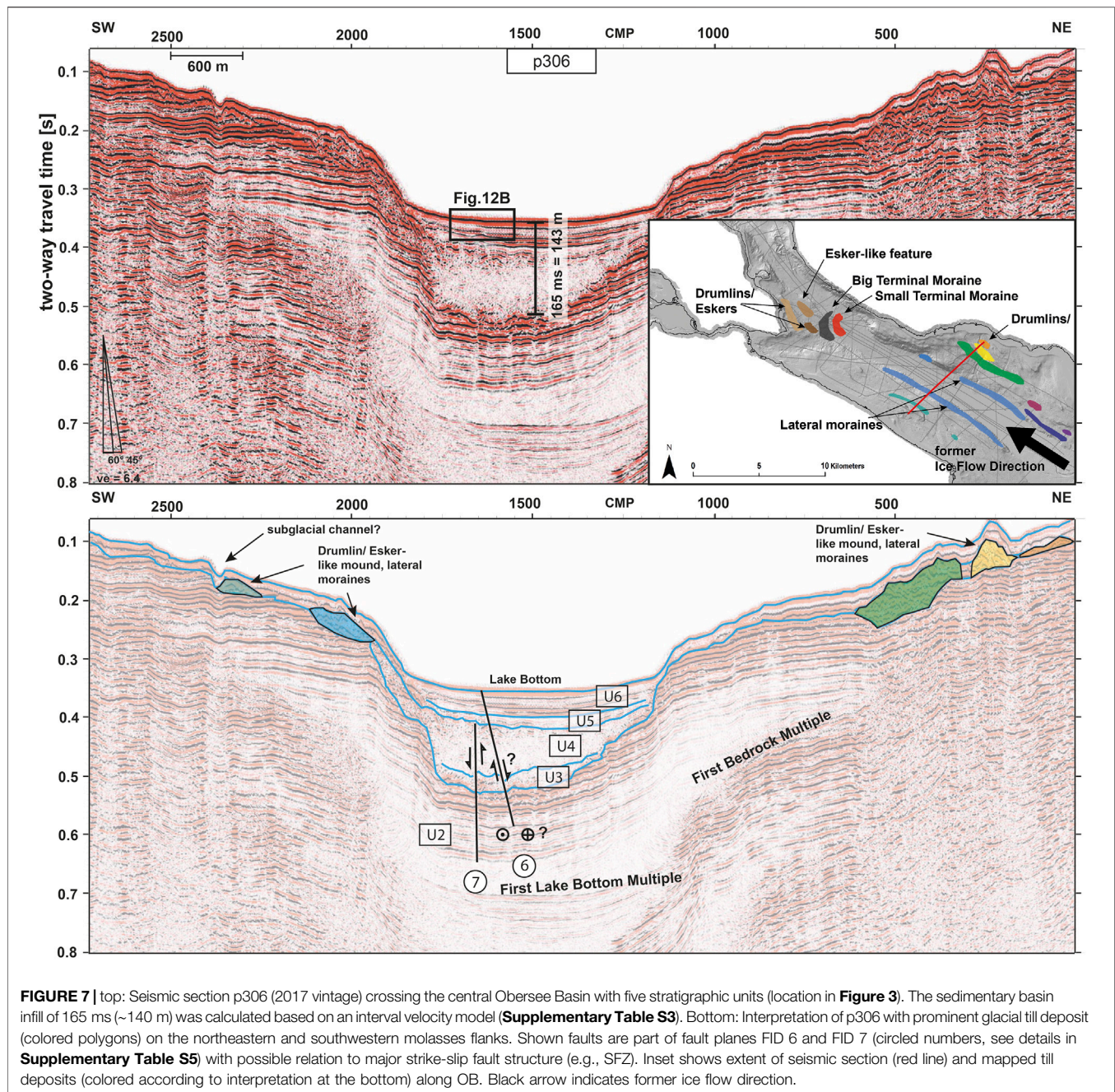
bedrock is covered by up to 227 ms of sediment, when approaching the Rhine Delta in the SE (**Figure 4**). Applying a velocity model, which is based on CTD measurements (conductivity, temperature, pressure/depth; Wong and Zhu, 1995) for the water column and on Normal-Move-Out (NMO) velocity picks from the multi-channel seismic data (see **Supplementary Table S3** for details), this translates into ~190 m of sediment. A similar sediment thickness is calculated for the delta-distal area, with a maximum at a localized bedrock depression with 200 ms (175 m) of deposits in seismic section prof01 (**Figure 4**). The trough geometry is illustrated by the exemplary crossline p306 (**Figure 7**). It is deepest close to the Rhine Delta, where bedrock topography reaches a local minimum of 578 ms (442 m depth with respect to a lake level of 395.6 m a.s.l. equal to -46.4 m a.s.l. see **Supplementary Table S3** for velocity model). At the transition between OB and UEB (5 km NW of Meersburg; **Figure 1**) 510 to 530 ms (433 m depth, -37.4 m a.s.l.) are observed. Even further to the NW, 547 ms (449 m depth, -53.4 m a.s.l.) are found in the central part of UEB. Note that greater bedrock depths in the central part of UEB, despite shorter twt values compared to the values at the Rhine Delta, are related to different thicknesses in glacial deposits and water column (see also *Bedrock Morphology and Overdeepening*). In UB, the Molasse

bedrock shows a local depression down to 270 ms (216 m depth, assuming lacustrine dominated infill and a constant velocity of 1,600 m/s, 179.6 m a.s.l.) close to Steckborn, but shows overall much shallower values for top bedrock. In the lack of drilling evidence, the bedrock depth values reported here strongly depend on the calculated interval velocities. Nevertheless, the expected uncertainty is in the range of a few percent only.

Glacial Deposits (U3 and U4)

The seismic facies of unit U3 is characterized by semi-transparent, chaotic facies at the top of the unit and shows medium-amplitude reflections at the base (SF3). U3 is predominantly occurring in the deep central part of OB and onlapping onto U2, but is hardly recognizable in UEB and UB. It is interpreted as a transition between bedrock (U2) and overlying purely glacial sequence U4, incorporating either older till deposits of pre-LGM (pre-Last Glacial Maximum) times or glacially ripped off and eroded Molasse bedrock pieces.

The seismic facies of unit U4 is characterized by transparent to semi-transparent chaotic facies (SF4), occasionally with short horizontal reflections similar to SF3. Toward the top of U4, the facies shows similarities to SF5. U4 forms the thickest unit of the Quaternary sedimentary infill in the central part of the OB



(**Figures 4, 7**), and likely contains diamict, glacial mud with dropstones, and a coarse gravelly base, as observed in onshore drill cores retrieved from subglacially eroded overdeepened bedrock troughs in the Alps (Buechi et al., 2017). U4 is onlapping onto U2 and in direct contact with it on the shallow northeastern and southwestern bedrock flanks. The combined thickness of U3 and U4 (**Figure 8E**) amounts in some local troughs to more than 270 ms (~240 m at 1800 m/s; **Supplementary Table S3**). U4 seems to pinch out towards the northwestern end of the UEB (**Figure 4**), which is misleading, since top of U4 cannot be picked and distinguished from overlying U5.

The bathymetric map reveals many morphologic features like streamlined lineations and hummocky structures related to glacial features reflecting paleo-ice flow of a retreating Rhine Glacier (Wessels et al., 2015). The seismic data reveal some of the glacial landforms hidden by lacustrine, pelagic sediments, which are undetectable on bathymetric data. These mound-like elongated subglacial landforms show a very similar facies to U4, with chaotic character, but significantly higher amplitudes (colored polygons in **Figure 7**). The inset in **Figure 7** displays the spatial extent of the mound-like subglacial landforms along the OB and its terminal features at the transition to the UEB.

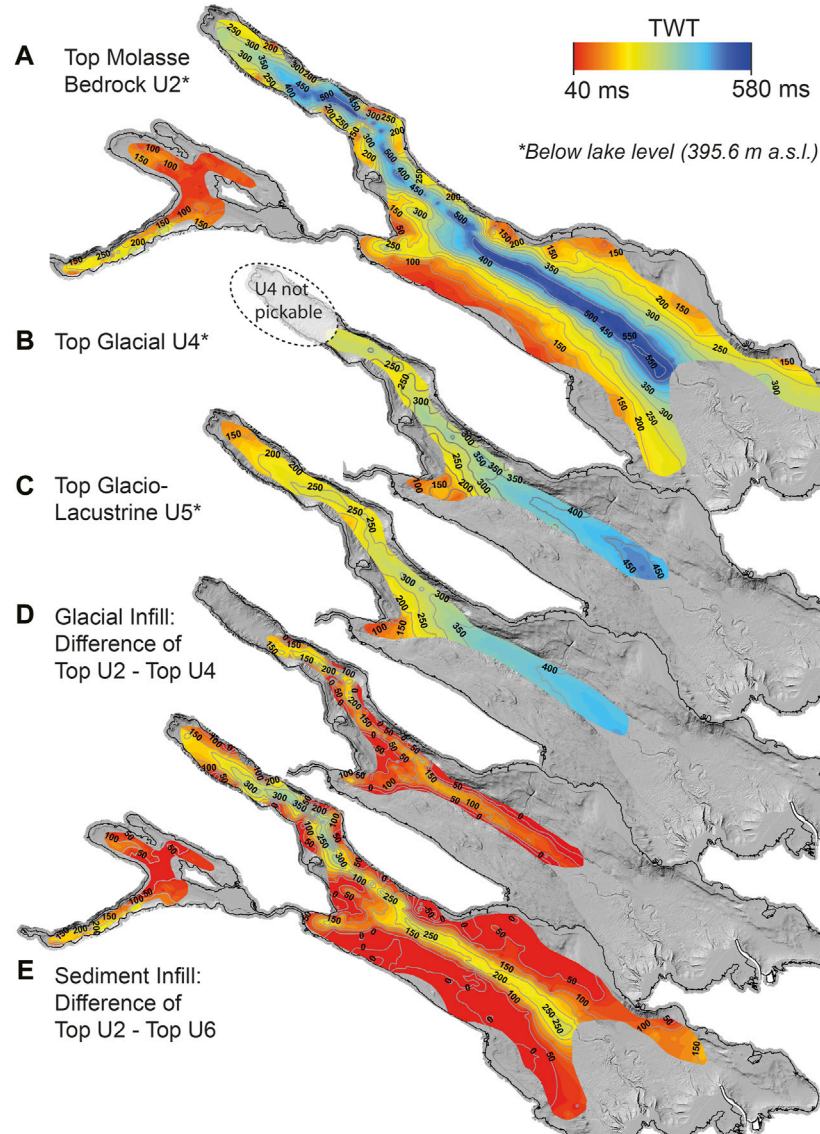


FIGURE 8 | A: Top of Molasse bedrock horizon (in twt) revealing pronounced overdeepening in the center of the OB and UEB with contour lines of bedrock (isochrone interval of 50 ms). B, C: Extent of glacial and glacio-lacustrine deposits corresponding to seismic facies unit U4 and U5. D, E: Thickness maps (50 ms intervals) showing the difference of top U2 minus top U4 and top U6, respectively. All data is shown in two-way travel time.

Glacio-Lacustrine and Lacustrine Deposits (U5 & U6)

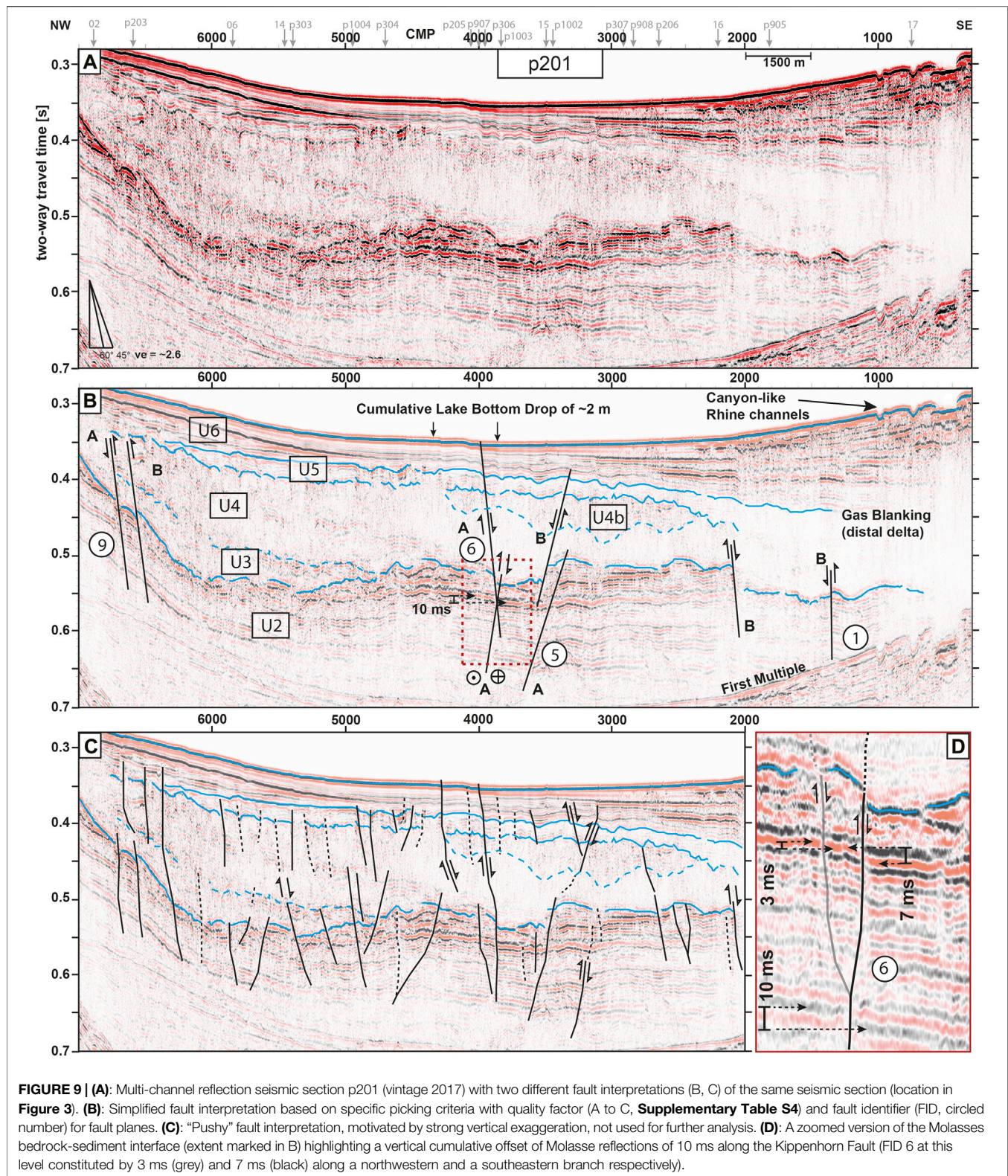
U5 shows transparent to semi-transparent chaotic facies at the base (transition from U4) with faint internal stratification, and medium amplitudes towards the top (SF5) of overlying U6 with a sharp amplitude increase (SF6). The hydroacoustic facies of this glacio-lacustrine unit indicates that it contains mostly sand and glacial mud, with coarse material at the base (Figure 4). U5 is limited to the deep central part of OB, can be traced in the entire UEB (Figure 8) and is onlapping onto U4 (Figure 7).

The seismic facies of unit U6 displays parallel, high-amplitude continuous horizontal reflections (SF6), with semi-transparent intercalated sections (sand to clay with intercalated turbidites). The sequence is characterized by an onlap geometry onto U5, occasionally also onto U2 where Molasse is on the rise to shallow

bedrock flanks northeast and southwest of the central basin (Figure 7). U6 is the shallowest unit and is interpreted as Holocene lacustrine sediments.

Lake-wide Fault Mapping Reliability of Fault Interpretation

The seismic recognition of faults depends heavily on the interpreter (Figures 9B,C), interpretation criteria, and the display parameters of the seismic data (e.g., amplitude gain or vertical exaggeration of the section). Therefore, a confidence scheme was introduced to evaluate the reliability of each interpreted fault, providing a qualitative value of confidence to the interpretation (Supplementary Table S4). While Figure 9C illustrates a “pushy” fault interpretation, a more conservative/



restrictive interpretation approach (**Figure 9B**) was chosen for the entire dataset, following the confidence scheme in **Supplementary Table S4**. Generally, faults were identified first

in the deeper parts of seismic lines (interpretation of discontinuities in the Cenozoic bedrock) and then traced upwards into stratigraphically shallower units (“bottom-to-top

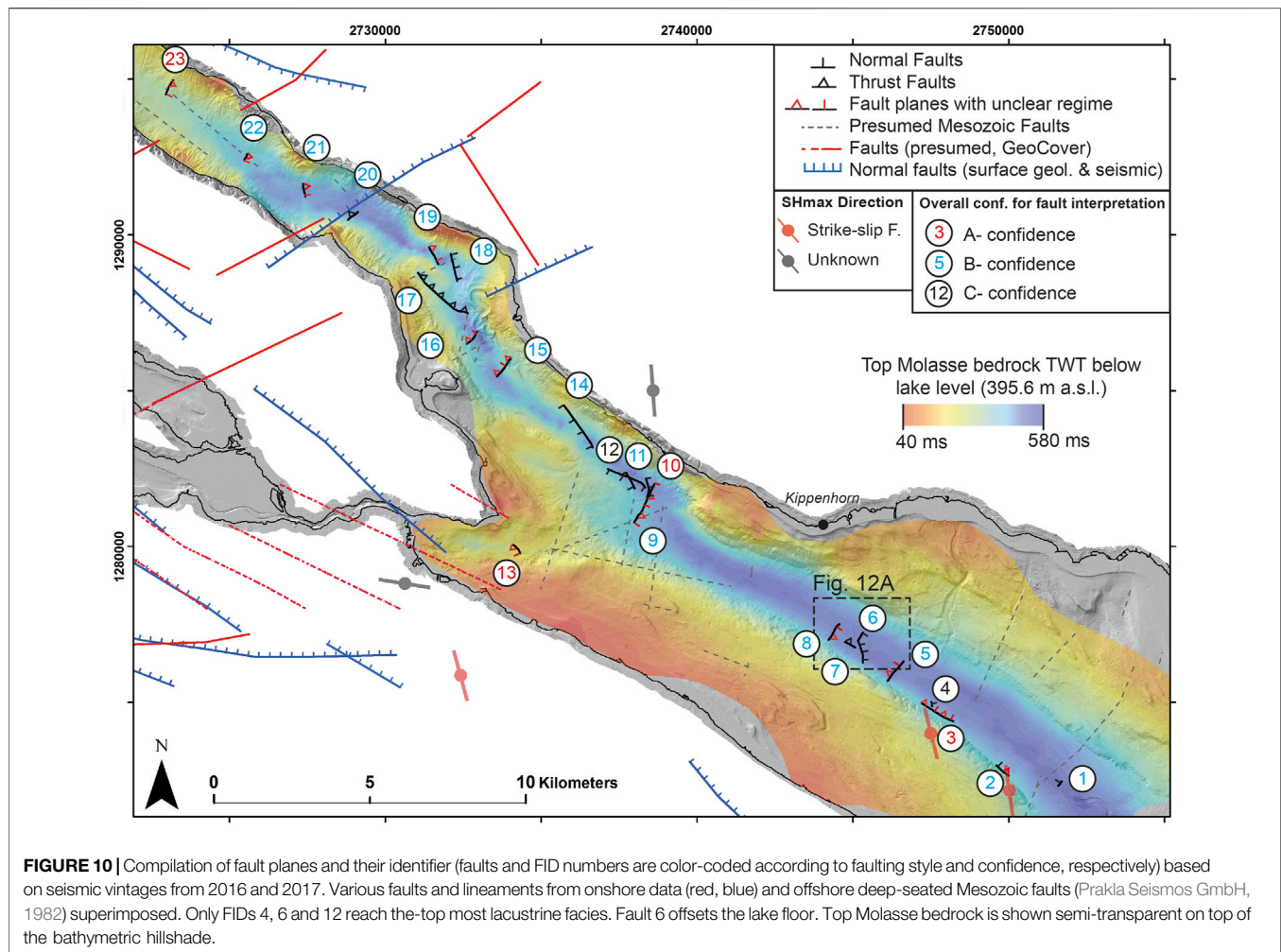


FIGURE 10 | Compilation of fault planes and their identifier (faults and FID numbers are color-coded according to faulting style and confidence, respectively) based on seismic vintages from 2016 and 2017. Various faults and lineaments from onshore data (red, blue) and offshore deep-seated Mesozoic faults (Prakla Seismos GmbH, 1982) superimposed. Only FIDs 4, 6 and 12 reach the-top most lacustrine facies. Fault 6 offsets the lake floor. Top Molasse bedrock is shown semi-transparent on top of the bathymetric hillshade.

approach”). Moderate and high confidence levels B and A require at least a partial offset of bedrock reflections and a continuous reflection offset traceable from bedrock into stratigraphically shallower units, respectively (see **Supplementary Table S4** for details). Lowest confidence level (C) was assigned, when a fault structure is likely due to vertically aligned amplitude anomalies indicative of gas accumulation, or when offset reflections are limited to the sedimentary lake infill (U3–U6), but no clear reflection offsets are recognizable in bedrock. Overall confidence of fault planes was based on the lowest ranked confidence of any contributing fault segments (**Supplementary Tables S5,S6**).

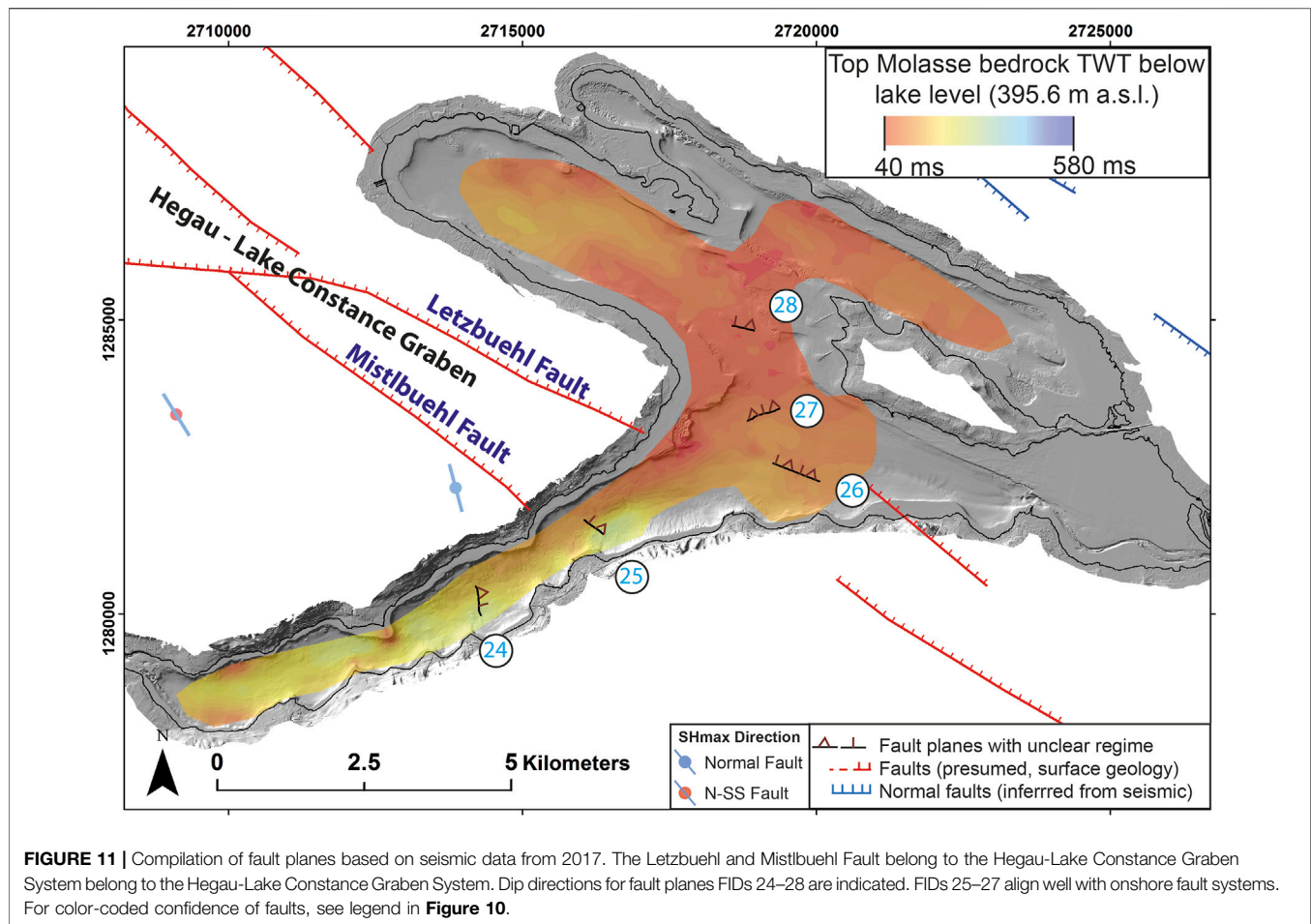
Linking Fault Sticks to Fault Planes

A total number of 154 single apparent fault sticks were mapped on the 2D seismic sections in the OB and UEB, and 39 fault sticks in the UB. Out of these 154 fault sticks, 60 could be linked across individual 2D seismic lines to form 23 fault planes in the OB and UEB (**Figure 10**). Similarly, in the UB, 12 fault sticks could be assigned to five fault planes (**Figure 11**). Every fault plane received an identifier (FID), and the bottom reach, top reach, minimum dip angle (apparent dip), horizontal and vertical extent, fault plane area, faulting style of contributing faults to

the fault plane, the overall faulting style and the overall quality/confidence (based on the lowest quality of any contributing fault) were systematically listed (**Supplementary Tables S5,S6**). The overall faulting style was defined by the majority of prevailing contributing faults; contradictory styles are marked as “unknown”. There is also a bias towards normal and thrust faulting, since horizontal movements are difficult to recognize in 2D seismic lines and can at best be anticipated through characteristic fault expressions, such as for instance flower structures (**Figure 9**).

The results of fault mapping are illustrated in **Figures 10, 11**. FIDs 1 to 23 belong to the OB and UEB, and FIDs 24 to 28 belong to the UB. To obtain a holistic view of the major fault planes, gridded 3D fault planes are reduced to 2D fault traces with observed dip direction and are superimposed on the Miocene Molasse bedrock map.

Generally, there are three different clusters of fault planes distinguishable in the OB and UEB (**Figure 10**), 1) in the deepest part of the OB (cluster 1: FIDs 1–8), 2) at the transition to the UEB (cluster 2: FIDs 9–14), and 3) in the UEB (cluster 3: FIDs 15–23). No fault-plane cluster can be identified in the UB. Lateral fault plane extension is defined by the outermost



fault sticks defining the fault plane, which in turn is dependent on the distance between individual seismic sections (grid density). Furthermore, the true vertical extension of individual fault planes to greater depth is most likely beyond the depth penetration of our seismic data. Therefore, here reported fault plane areas represent minimum estimates. Lacking a detailed velocity model, fault-plane areas in the UB could not be calculated.

All of the interpreted fault planes root in Molasse bedrock, apart from FID 4, which only roots shallower in U3. Most of the mapped faults penetrate into U4 or U5 but, only FIDs 4, 6 and 12 reach the topmost lacustrine sediments in unit U6. FID 6 additionally shows a significant vertical lake-bottom offset of ~2 m (**Figures 4, 7, 9, 12**). While most fault planes are defined by fault sticks interpreted on two to three seismic sections, FID 6 is defined by five different seismic sections, all consistently showing a normal faulting style. Given the comparably strong robustness of this fault's seismic interpretation and its expression on the lake bottom suggesting very recent activity, it was selected for further investigations.

Detailed Characterization of Fault Plane 6—The Kippenhorn Fault

In order to spatially constrain and further investigate the activity of bedrock-rooted FID 6 (hereafter termed Kippenhorn Fault, see

Figures 4, 9), six high-resolution single-channel seismic lines were acquired across the NNW-SSE striking and ENE dipping fault plane (minimum dip angle 33°), supplemented by a transect of five short cores along seismic section BO19-01 (**Figure 12**). A bathymetric profile parallel to BO19-01 shows a morphologic step of 2 m, as previously noticed in multibeam data (Wessels et al., 2015) and seismic section p201 (**Figure 9**) likely representing a surface rupture of the fault. The cores were taken at this morphologic step and in ~100 m equidistance from northeast to southwest across the fault (**Figure 13**) to investigate the Kippenhorn fault activity based on off-fault evidence. 13 different turbidite layers (A–L) were identified in the five transect cores and seven of them could be correlated across all cores. Their individual thickness was measured in percentage relative to the most southwestern core and plotted against distance along the transect (**Figure 13** top). Across the fault from SW to NE, a linear stratigraphic thickening of 125–175% (0.1–2.1 cm) is observed. Turbidite B, however, shows a thickness increase by 450% (20.5 cm) from the most southwestern (BO19-113, Kippenhorn Fault footwall) to the most northeastern core (BO19-115, Kippenhorn Fault hanging wall), fitting an exponential stratigraphic thickness increase across the fault. Furthermore, seven sufficiently thick turbidites (T1–T7) were identified with their transparent seismic facies in the high-resolution seismic line BO19-01 and correlated across the fault

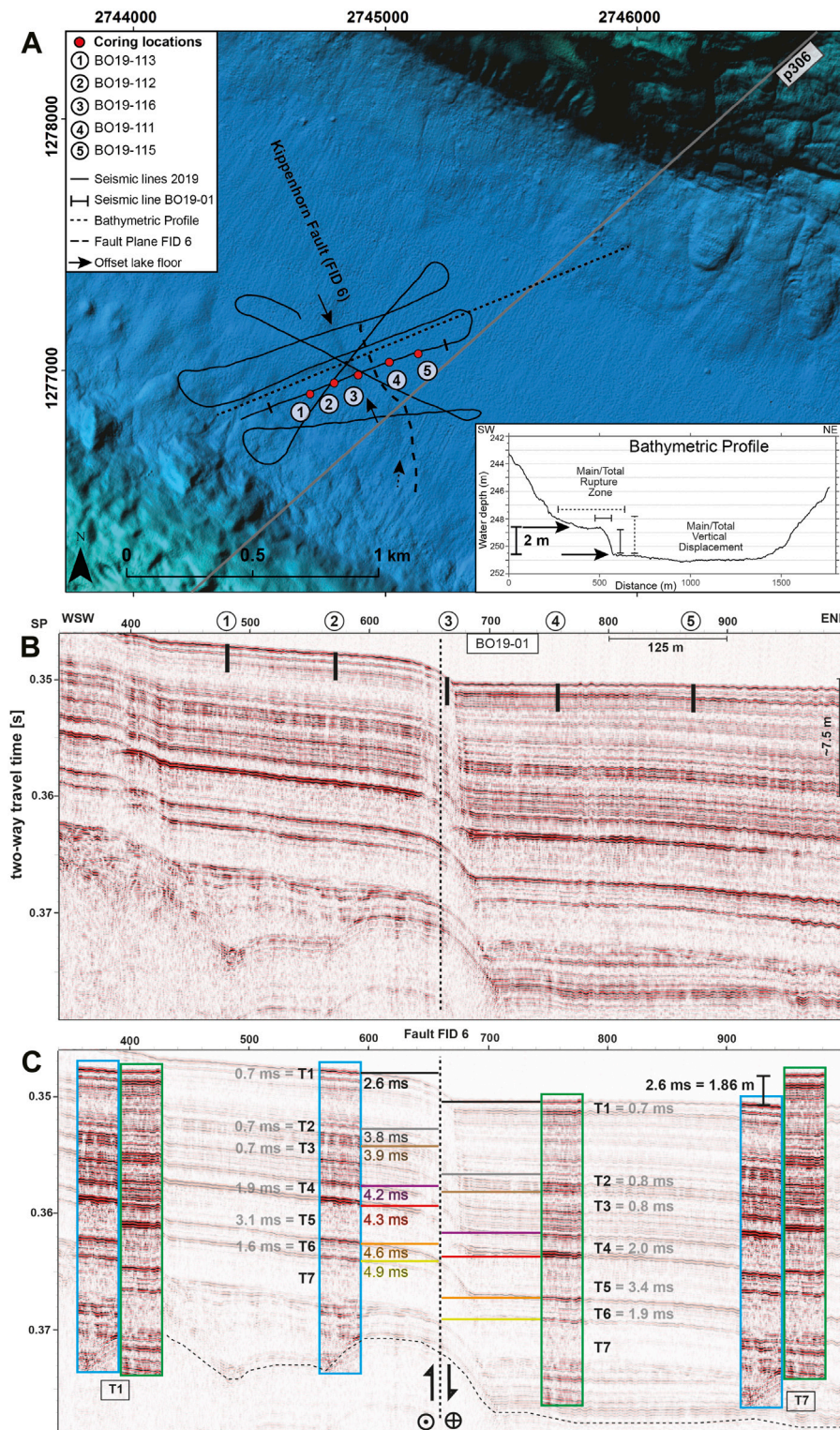


FIGURE 12 | (A): Bathymetric map with single channel 3.5 kHz seismic survey lines from 2019 for fault plane FID 6 characterization (black arrows mark lake bottom expression). The trace of fault plane FID 6 (black dashed line) is projected onto the lake bottom from 400 ms twt depth. Locations of short cores (1–5) are indicated. See **Supplementary Table S7** for more details. Seismic section p306 is shown in **Figure 7**. Extent of the figure is shown in **Figure 10**. Inset: Bathymetric profile highlighting lake-bottom offset. **(B):** Seismic section with short core locations superimposed. **C:** Turbidite (T1–T7) correlation across the fault plane FID 6 and offset comparison of footwall with hanging wall (color-coded numbers). Thickness of T1–T7 on either side of the fault is given in grey numbers. Cumulated sedimentation difference between foot- and hanging wall amounts to ~2 m (based on a water column sound speed of 1,428 m/s, see **Supplementary Table S3**) at the lake bottom, indicative for the power of turbidities to level out offsets over time. **Figures 4, 9** show the deeper structure of this section (dotted line). Horizon offsets (color-coded twt) increase with depth.

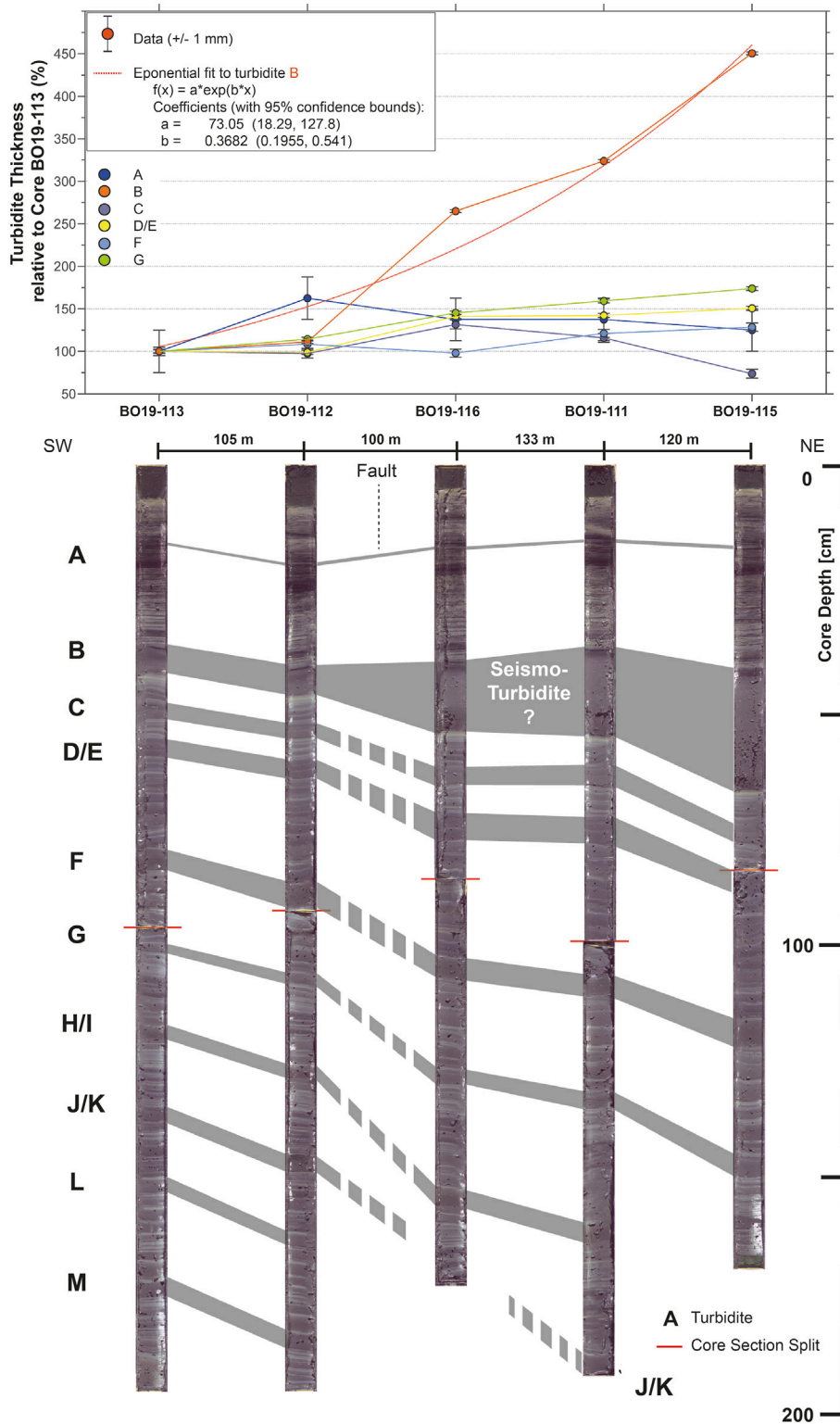


FIGURE 13 | Collection of short core transect across fault plane FID 6 (see Figure 12, Supplementary Table S7 for location and details). Thickness development of identified turbidites A to M is plotted above. Errorbar is based on a thickness reading error of ± 1 mm, expressed as percentage of total turbidite thickness. Turbidite B expresses an exponential thickness development across the fault possibly indicative for fault activity. Other turbidites show linear thickness increase across the fault.

via correlation polygons (**Figure 12**). The cumulative turbidite thickness difference across the fault amounts to 2.6 ms (1.86 m, for 1,428 m/s) at the lake bottom, agreeing with independent step height measurements (~2 m) from multibeam bathymetry. Note that at greater depth, the Kippenhorn fault shows a cumulated vertical 10 ms offset of Molasse reflections (13.5 m based on 2,700 m/s interval velocity) constituted by two fault branches (see **Figure 9D** at ~550 ms twt: northwestern branch 3 ms, southeastern branch 7 ms). This ~10 ms offset of the Kippenhorn fault at the level of the Molasse decreases from 4.9 ms (T7) to 2.6 ms (T1, **Figure 12C**) at the lake bottom and shows a regressive offset development.

DISCUSSION

Implications for Seismic Stratigraphy and Paleoenvironment

Bedrock Morphology and Overdeepening

Previous seismic campaigns (Müller and Gees, 1968; Finckh et al., 1984) distinguished three seismic units within Lake Constance: The lowermost one was interpreted as Molasse bedrock (Cenozoic), followed by Late Pleistocene heterogeneous glacial material (till), which is overlain by the uppermost unit consisting of postglacial (Holocene) fine-grained, well-bedded lake sediments. Our investigation, based on new seismic imaging techniques and a multi-vintage approach, allows distinguishing at least five major seismic units in OB and UEB (U2-U6) and four units in UB. Furthermore, the previous suggestion of ~100 m of Holocene sedimentary infill (Müller and Gees, 1968; Finckh et al., 1984) in the central basin of OB seems to underestimate the thickness of the infill. In the same area of the northwestern OB, up to 200 ms (175 m, see **Supplementary Table S3** for velocity model) of sediment are mapped, whereas even up to 280 ms (~240 m) of sedimentary deposits are identified in the Rhine Delta distal area (**Figure 8**). Locally in the UEB, Quaternary sediment thicknesses of up to ~370 ms (~300 m) are observed, accompanied by relatively shallow bathymetric values compared to the central OB. The Quaternary infill in UB amounts to ~230 ms (~195 m, assuming a glacio-lacustrine dominated infill with an average velocity of 1700 m/s) in its deepest part close to the outflow of the Rhine River. Such Quaternary overdeepened troughs are not limited to the lacustrine environment and have been reported from several deep drilling campaign onshore in the NAFB (e.g., Buechi et al., 2018; Huber et al., 2020).

A maximum overdeepening of 578 ms (442 m depth with respect to the current fluvial base level of 395.6 m a.s.l. equal to -46.4 m a.s.l.) close to the Rhine Delta in the OB and 547 ms (449 m depth, -53.4 m a.s.l.) in the central part of UEB results from subglacial erosion below today's sea level. This is generally in good agreement with observations in other perialpine lakes north of the Alps (e.g., Finckh et al., 1984; Preusser et al., 2010; Fabbri et al., 2018). While the Southern Alpine deep incision (Finckh, 1978) may be caused either by subglacial activity (Winterberg et al., 2020) or by the Messinian drawdown of base level (e.g., Cazzini et al., 2020), overdeepenings north of the Alps are primarily attributed to a glacial origin (Preusser et al., 2010). During the Last Glacial

Maximum (LGM), the Rhine Glacier's ice elevation above the Lake Constance area was at ~1,000 m a.s.l (Bini et al., 2009), indicating an ice thickness of ~1,500 m. During the Quaternary, several glacial advances coupled with the erosive power in the subglacial domain created overdeepenings and shaped the perialpine realm (Preusser et al., 2010; Reber and Schlunegger, 2016; Magrani et al., 2020). The overdeepening in Lake Constance can likely be attributed to multiple supporting factors like 1) lithological bedrock control (erosion-sensitive bedrock), 2) tectonic predisposition (weakening of underlying bedrock through an extensive fault system) and 3) channelized subglacial erosion (Preusser et al., 2010; Dürst Stucki and Schlunegger, 2013). It appears that the latter two factors, with a dense network of faults in the central OB and UEB (see *Lake-wide Fault Mapping*, **Figure 10, 11**), combined with focused subglacial erosion dominate the Lake Constance bedrock morphology and its present bathymetry. The overdeepening in the UB is significantly lower than in the OB and UEB with a maximum depth of 280 ms below lake level in the most western part. The smaller overdeepening is likely related to 1) the reduced subglacial erosional power of the Rhine Glacier further away from its accumulation area and 2) the reduced amount of faults pre-conditioning and weakening the local bedrock, making it less susceptible to erosion.

Traces of the Rhine Glacier

The transition from Molasse bedrock to glacial deposits is marked by the sporadically mappable unit U3 in the OB, which we interpret as indicative for possibly older pre-LGM deposits or mechanically broken-off chunks of bedrock. This resembles Lake Annecy and Lake Le Bourget (Van Rensbergen et al., 1998; van Rensbergen et al., 1999) as well as Lake Thun, (Fabbri et al., 2018), which likely host remnants of pre-LGM sediments that have not been fully removed by the last glacial advance. Generally, glacial deposits (U4) dominate the central part of the OB and UEB, and could neither be recognized on the shallow water bedrock shoulders in the OB, nor in the UB, due to their absence or the insufficient resolution of the seismic datasets. However, mound-like elongated subglacial landforms on the flanks of the OB could represent accumulations of the basal lodgment till (lineaments or "overdeepened drumlins") or subglacial channel fills (e.g., eskers/lateral moraines, **Figure 7**). The northeastern area of the OB shows a higher preservation potential for these features than the southwestern bedrock shoulder. While the thick deposits of U4 clearly mark the onset of loss of ground-contact of the retreating Rhine Glacier, the deposition of glacio-lacustrine sediments of unit U5 indicate a disintegrated and retreating glacier into inner-alpine areas. The global LGM (Mix et al., 2001; Clark et al., 2009; Hughes et al., 2013) coincides fairly well with the maximum reach out of Alpine piedmont glaciers into the northern foreland, so that we attribute U4 to LGM times. The terminal moraine like features at the transition between the OB and UEB are, in contrast to the basin parallel eskers/lateral moraines, covered by U4, indicating that they are older than the LGM or that they mark the onset of a recessional phase with a locally fluctuating glacier front (e.g., Monegato et al., 2007).

Implications of Active Faulting in Lake Constance

Age and Interpretation of Faulting

In the context of this investigation, the minimum age of a seismically interpreted fault is defined by the vertical reach of the fault (the shallowest penetrated stratigraphic unit). All fault planes in the OB, UEB and UB root in Molasse bedrock (U2), except FID 4, which roots in U3. Most penetrate into U4 or U5 in the OB and UEB, and only FIDs 4, 6 and 12 reach the topmost lacustrine sediments in unit U6, and hence show the most recent activity (Holocene). With clear evidence for Quaternary activity, all of the 28 faults interpreted herein must be regarded as being active.

The numerous active faults within Lake Constance, identified despite a rather conservative seismic interpretation approach, are in contrast to very few such observations for onshore faults (e.g., Wiemer et al., 2009). This showcases the enormous fault detection potential of lake deposit archives for regions characterized by strong Quaternary landscape overprint (both geologically/geomorphologically and anthropogenically). First and foremost, this raises the question what processes have driven the formation of these active structures? As the presented faults in Lake Constance root deep in Molassic bedrock, sedimentary compaction is an unlikely source for their development. Given the obviously intense glacial erosion of the Lake Constance basin, postglacial rebound could be considered as possible trigger mechanism for seismogenic fault reactivation and (Wood, 1989; Ustaszewski et al., 2008; Mey et al., 2016) cannot be entirely excluded as one possible driving mechanism. Nevertheless, considering the very good correlation of the presented faults within Lake Constance with onshore tectonic structures (see following section), we consider tectonic crustal stresses related to the latest stage of Alpine orogeny also as being responsible for the region's seismicity (Kastrup et al., 2004; Mock and Herwegh, 2017; Houlié et al., 2018; Dal Zilio et al., 2020; Diehl et al., 2021) as the main driver of the active faulting observed in Lake Constance.

Correlation of Lake Faults With Onshore Fault Systems and Control on Quaternary Basin Evolution

In the UB, most of the observed fault sticks (39) do not reach beyond bedrock. This impression may be misleading, as strong multiples induced by gas-rich sediments, make seismofacies units and fault's dissecting difficult to discern. In any case, the few faults in the UB actually reaching beyond bedrock into shallower facies all occur in the western part, possibly indicating a more recent fault activity of this region, at least since LGM. The fault planes (FIDs 25–26) align well with onshore mapped fault systems. The NW-SE striking FID 26 seems to roughly connect with onshore faults NW and SE related to the southern continuation of the Randen/Letzbuehl Fault (Figure 11) and shows the same NE dip direction. Fault plane FIDs 24 and 25 may be part of the same normal fault system lying in prolongation of the Mistlbuehl Fault and a projected fault southwest of it (Figure 11). Their orientation with respect to the current tectonic stress regime ($SH_{min} = NE-SW$) is compatible

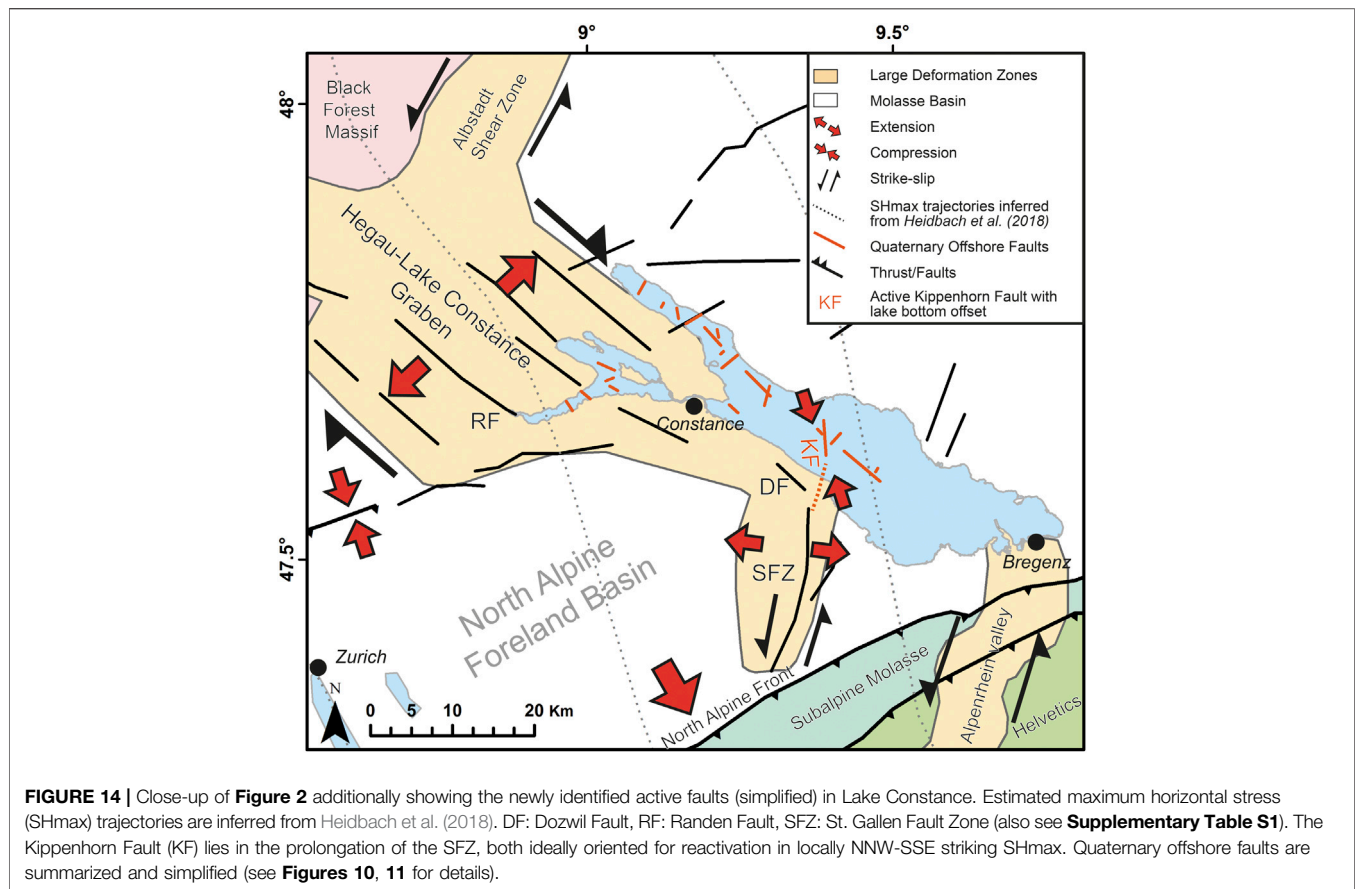
with reactivation in normal to transtensional faulting mode (Diehl et al., 2020). At least in the case of the Mistlbuehl Fault, a pronounced Quaternary graben recognized in seismic data indeed suggests Pleistocene activity of this type of faults (Figure 5). FID 25 appears to be in the center of Quaternary graben structure. Finally, FID 27, striking NE-SW runs parallel to the UB fitting to a presumed fault underneath this lake peculiarly orientated parallel to major regional faults reported further to the west (Madritsch et al., 2018; Roth et al., 2010).

Most of the faults in the UEB and the OB also trend NW-SE, parallel to the Hegau-Lake-Constance graben (Egli et al., 2016; Ring and Gerdes, 2016). In addition, NNE-SSW to NNW-SSE are commonly recorded, incl. the Kippenhorn Fault (*Origin, Timing and Kinematics of the Kippenhorn Fault*). Similarly oriented faults are well known around the lake, most importantly the St. Gallen Fault south of it (Heuberger et al., 2016).

The prominent bedrock trough following the long axis of Lake Constance from the Rhine river inflow, along the OB to the most northwestern extent of the UEB is frequently disturbed in its course (Figure 10). Its course changes seem to correlate with the fault plane clusters 2 (FIDs 9–14) and 3 (FIDs 15–23). Cluster 2 coincides with Mesozoic deep-seated faults from offshore seismic data from the 80s (Prakla Seismos GmbH, 1982). Especially cluster 3 agrees well with existing offshore (e.g., FIDs 15 and 16) and onshore (e.g., FID 20) faults. The spatially highly variable bedrock topography strongly suggests a dominating fault control, favored by subglacial erosion, explaining the sudden turns and bends of the deepest bedrock channel. Cluster 1 (FIDs 1–8) also relates well with offshore faults and lies in direct prolongation of various well-constrained fault systems (St. Gallen Fault Zone (SFZ) Roggwil Fault Zone (RFZ) in Figures 1, 14). While the RFZ is limited to the Mesozoic strata and the Upper Freshwater Molasse, FID 6—the Kippenhorn Fault offsetting the lake bottom (Detailed Characterization of Fault Plane 6—The Kippenhorn Fault) seems to be associated with the seismically active SFZ (see next section).

Origin, Timing and Kinematics of the Kippenhorn Fault

Turbidites, as developed around the Kippenhorn Fault, can generally be triggered by several processes and are often used as a tool for paleohydrologic reconstructions and the recurrence of floods (e.g., Gilli et al., 2013; Kremer et al., 2015a). Earthquakes have also been shown to trigger subaquatic slope failures causing turbidity currents, what makes them suitable for paleoseismology in the form of secondary evidence (Goldfinger, 2011; Moernaut et al., 2014). Especially where outcrops and primary earthquake evidence is not accessible, turbidites in lacustrine environments are commonly used to assess the frequency of earthquake events (Schnellmann et al., 2006; Goldfinger et al., 2012). More recently, it has been shown that co-seismic turbidites as indicator for growth faults with significant thickness changes across a fault (Bouroullac et al., 2004) can be used to reconstruct the activity of seismogenic faults (Beck et al., 2012; Gastineau et al., 2021). Such seismo-turbidites, directly related to the rupture of a fault structure, cannot be triggered far from the ruptured fault segment (McHugh et al., 2014).



Three possible scenarios may explain the origin of the morphologic step associated with the Kippenhorn Fault in Lake Constance.

1) Glacial origin: A post-LGM glacio-topographic step caused by till morphology is formed in the basin and pelagic sediments and turbidites level out this inherited offset over time, a still ongoing process. The exponential stratigraphic thickening of turbidite B in the core transect across the step, which is preceded and succeeded by linear stratigraphic thickening, in combination with the identified turbidites seen in the high-resolution seismic data, however, questions the pre-existence of the step. Furthermore, deeper multi-channel reflection seismic data does not imply the existence of a glacially originated step (**Figure 7**) and rather supports the direct link to a bedrock-rooted fault structure that periodically reforms and sustains the offset at the lake bottom.

2) Tectonic origin: The morphologic step is retracing a bedrock fault that is currently in the process of being levelled out by ongoing sedimentation. Moreover, the bedrock fault structures (**Figure 9**) are reminiscent of a flower structure that is typical for strike-slip faulting regime that would be expected for the NNW-SSE striking Kippenhorn Fault in the present-day stress regime.

3) Tectonically active origin: The morphologic step is part of an episodically active, possibly seismogenic, bedrock-rooting fault zone. Following a fault-related rupture of the lake

bottom, the turbidites of varying thickness are deposited on both sides of the Kippenhorn Fault and the lake bottom becomes flattened over time (**Figure 12**). Further pelagic sediments are deposited evenly on both sides of the fault until another phase of activity occurs and this process is repeated.

Overall, combined datasets from multibeam bathymetry, multi-channel reflection seismic data from two different vintages (2016, 2017), high-resolution single-channel data from two different vintages (2015, 2019), and a coring transect with five cores support the interpretation that the ~2 m high morphologic step is related to an active bedrock-rooting fault plane (Kippenhorn Fault) in the center of the OB in Lake Constance. An age assignment of turbidite B can be attempted through the identification of historical flood events (Wessels et al., 1999; Wessels, 2003). The correlation of the sediment cores (**Figure 13**) shows a prominent beige layer below turbidite B, which is visible in all cores. This layer is dated to 1893 CE \pm 2 years (Wessels, 2003) so that turbidite B could have been deposited around 1895/1900 CE, unless the base was highly erosive. During this period, there was no significant flood event (LUBW, 2011), implying that turbidite B is the result of a local mass movement possibly originating on the southern lake slope. However, no indication of a scarp or a deposit related to such a recent mass-movement event appears on the bathymetric data. Alternatively, the brown-gray layer ~3 cm above the prominent layer B possibly dates to 1918 CE (Wessels, 2003),

which would suggest that turbidite B was deposited ~1910 CE, when the Rhine River had a major flood event (Gilli et al., 2003). This 1910-layer is well known from a high number of sediment cores and regularly used for dating purposes in Lake Constance. Such hyperpycnal flows (Sturm and Matter, 1978), however, can hardly form such an isolated thick layer 20 km away from the river mouth. Therefore, layer B is most likely not a flood-related event, but is rather a mass-movement turbidite deposit, which could be of seismic origin. Two possible time periods for the formation of the prominent, presumably mass-movement related turbidite layer B are likely: period 1895 to 1900 CE or around the year 1910 CE. In fact, both periods qualify for earthquakes as potential triggers (Figure 1, inset) and being indicative of the fault's most recent activity. A historical earthquake of magnitude 5.5 occurred in southern Germany in 1911 and led to numerous damages of infrastructure. In any case, the striking exponential thickness increase of turbidite B across the Kippenhorn Fault possibly dates the last activity of the fault plane, and hence could indicate that a small-scale local earthquake caused the reactivation of the fault.

However, one has to strictly differentiate between events that do, and those that do not rupture the surface, moreover between strike-slip faults that do not necessarily show surface-rupturing at all. The last activity of the fault (~100 years ago) did not release enough energy to create a measurable increase of the vertical offset. An $M_w > 6$ event several hundreds to thousands of years ago is more likely to have caused the lake bottom offset (surface-rupturing) under the assumption the event involved a vertical faulting component. Since Holocene deposits (U6) are clearly affected by at least one larger event, an upper boundary for the age constraint of ~11.6 ka for the last major active phase seems likely.

Since the Molasse bedrock underneath Lake Constance has been affected by Alpine foreland deformation ever since its deposition in Miocene times (Egli et al., 2016; Heuberger et al., 2016), we interpret the observable subsurface offset in the Molasse bedrock of 10 ms (13.5 m) as a cumulative one that has likely resulted from several displacement events. The 13.5 m offset is measured within the Molasse stratigraphy, and its top is less clearly resolved on the seismic data (Figures 9B–D) as it has been eroded by multiple glaciations. Hence, the 13.5 m offset might be created, at least partially, during pre-LGM times. In the upper part of the Quaternary sediments (U6, U5), this value gradually decreases upsection from 4.9 ms (3.7 m; at T7) to 2.6 ms (1.86 m; at the lake floor, Figure 12C). This may be related to two different scenarios:

1) One or several earthquakes at the Kippenhorn Fault occurred between post-LGM times and the deposition of T7 causing a cumulative offset of at least 4.9 ms (Figure 12C). Afterwards, several turbidites level out the offset across the fault during a period without major, offset-renewing earthquakes. According to this scenario, the 2 m lake-bottom offset observable today is a remnant of a previous stronger and more seismically active phase, or a phase dominated by pure strike-slip faulting not resulting in pronounced additional vertical offset.

2) Every single turbidite (T1–T7) is related to an offset-renewing earthquake and co-seismically deposited. To

evaluate whether T1–T7 are related to local earthquakes, to flood events, or to more regional far field earthquakes, an accurate age-depth model covering several tens of meters would be required. In any case, the 2 m lake bottom offset observable today would represent an expression of the fault's most recent activity that involves a significant normal faulting component. It would be of particular interest to compare if T1–T7 match the temporal clustering of off-fault paleoseismic evidence suggesting several strong earthquakes and distinct phases of increased activity between 300–600, 1,400–1700, 2,200–2,500, 3,000–3,600, 6,200–7,000 and at around 9,500–9,900 years cal BP (Kremer et al., 2020).

The depth coverage of the various datasets (cores 2 m, high-resolution seismic data: ~30 m, multi-channel reflection seismic air gun data: ~400 m) and their corresponding vertical and spatial resolution are not sufficient to determine any evidence for clear co-seismic surface rupturing in the most recent depositional history (T1–T7). More high-resolution seismic data including air gun data would be required in combination with long cores to fully resolve which scenario prevails.

For a detailed kinematic analysis of the Kippenhorn Fault, relative kinematics on 2D seismic sections were mapped (e.g., Figure 9B,C) showing sets of normal and thrust faulting. The sets of normal faults dominating and surrounding the Kippenhorn Fault were observed in several parallel 2D seismic lines, allowing for a 3D interpolation of the fault, indicating a 3D negative flower structure reminiscent for strike-slip faulting with a normal faulting component. The consideration of recent stress indicators (focal mechanisms, drilling-induced fractures, borehole breakouts Heidbach et al., 2018) and surface data suggests that the NNW-SSE striking Kippenhorn Fault is ideally oriented to be reactivated in sinistral strike-slip fashion (Figure 14). This is analogous to the St. Gallen Fault Zone, which was reactivated in the induced 2013 earthquake in almost pure sinistral strike-slip mode (Diehl et al., 2017). We regard this kinematic similarity as indicative for a possible linkage of the Kippenhorn Fault with the SFZ.

Implications for Seismic Hazard

Seismic hazard analyses for any given area require an assessment of the earthquake potential including estimates of fault rupture parameters to quantify the future earthquake potential (Wells and Coppersmith, 1994). The rupture parameters in turn are related to earthquake magnitude. Commonly considered rupture parameters in this regard are fault length and displacement (Chinnery, 1969).

The offshore fault planes FIDs 1–28 are all smaller than 1.66 km². The longest fault is ~2.1 km long (FID 17). The youngest FIDs 4, 6 and 12 in the OB have fault plane lengths between 150 m and 1.4 km. The Kippenhorn, with particular strong evidence for Holocene activity, deserves special attention. This fault is ~1,100 m long. One single rupture event involving the entire related fault plane area of 0.54 km² would produce a $M_w = 4.3 \pm 0.1$ earthquake (Stirling et al., 2002) assuming revised and instrumental based regression curves (Wells and Coppersmith, 1994; Stirling et al., 2002). Using more recent earthquake-scaling relationships from geodetically derived slip

distributions, this fault plane area would produce a M_W 4.6 ± 0.2 when activated in strike-slip mode (Brenngman et al., 2019). Taking the ~ 240 m length of the surface expression of the Kippenhorn Fault from the bathymetric dataset into account (distance between solid black arrows in **Figure 12**), a $M_W = 4.8 \pm 0.1$ earthquake might have been responsible for the last reactivation using the regression curves for surface-rupture lengths (Stirling et al., 2002). These first order estimates include only the main rupture zone (**Figure 12A** inset) and do not include additional branches of the total rupture zone. Furthermore, the true vertical and lateral extension of the Kippenhorn fault goes beyond the seismic grid coverage and depth penetration, why these magnitude estimates are minimum values. Typical comparable earthquakes of $M_W \sim 5$ do not show surface rupturing, unless their hypocenter is very shallow, as in Le Teil, France (M_W 4.9 with 15 cm vertical offset, Ritz et al., 2020). Neighboring faults (e.g., FID 5, **Figure 9B**) may likely be part of the overall flower structure, doubling the affected total fault rupture zone. As outlined above, the Kippenhorn Fault shows the same orientation, dip direction and faulting style as the St. Gallen Fault Zone, so that a connection to the SFZ seems likely. The flower-structure fault pattern around the Kippenhorn Fault (**Figure 9**) indicates that a strike-slip faulting component of the fault plane is likely, similar to the present-day faulting regime inferred for the SFZ (Heuberger et al., 2016). Moreover, the Kippenhorn Fault is ideally oriented in today's stress regime for being reactivated in strike-slip mode, so that a sequential triggering of the fault zone through the past seems likely. A faulting event involving the SFZ as well as the Kippenhorn Fault, extends the fault length to 30 km and may cause ground shaking exceeding previously known intensities ($M_W = 4.1$, epicentral intensity V, 3 km north of Arbon, 1936 CE, $M_W = 4.7$, epicentral intensity VI, Arbon, 1720 CE, $M_W = 5.1$, epicentral intensity VII, 12 km northwest of Arbon, 1771 CE) in this area, also in the case of just partial fault reactivation. Considering simultaneous activation of the Kippenhorn Fault and the SFZ, the 30 km long fault would be capable to release the energy of a $M_W = 6.7$ earthquake, when triggered in strike-slip mode (Brenngman et al., 2019). Similarly, if we assume a single event to be responsible for the vertical lake bottom offset of 2 m, a magnitude = 6.6 is expected, when triggered in normal faulting mode (Brenngman et al., 2019). These values can be considered as upper-bound magnitudes.

Generally, earthquakes with $M_W > 6$ at shallow crustal depths (~ 10 km) imply a co-seismic surface rupture length of ~ 30 – 40 km. Such severe and extensive evidence of surface rupture from previous events is not observable today, indicating earthquakes with ages of several thousand years and a dominantly lateral offset, with minor vertical displacement of the ground surface. The SFZ might be a good candidate as a potential source for a very similar event. In any case, i.e., a single or cumulative offset, the expected magnitude of a Kippenhorn Fault earthquake is clearly above known events from the earthquake catalogue (Fäh et al., 2011) indicating a higher seismic hazard than previously known. This reveals the necessity to further investigate the Kippenhorn Fault and its continuation to the south in on- and offshore areas and hence its

potential linkage to the SFZ. Furthermore, the SFZ in particular should be further investigated in order to verify or falsify the evidence for repeated recent surface faulting events along the major fault zone. This demonstrates the importance to incorporate paleoseismological studies into regional seismic hazard assessments.

CONCLUSION

Newly acquired, multi-vintage reflection seismic data of the deep subsurface of trination Lake Constance reaches Mesozoic and Molassic strata. Deep erosional incisions into the Molassic bedrock filled with thick Quaternary deposits reveal a complex morphology and infill indicative for multiple glacial advances. In the northwestern part of the Obersee Basin (OB), up to 175 m of Quaternary sediment are present, and even up to 240 m of sedimentary deposits near the center of the basin (**Figure 4**). In the Ueberlingen Basin (UEB), locally, up to ~ 300 m of sedimentary infill is observed in relatively shallow areas. The sedimentary infill in the Untersee Basin (UB) amounts to ~ 200 m in its deepest part close to the outflow of the river Rhine. A minimum overdeepening of 442 m (-46 m a.s.l.) with respect to the current fluvial base level in the OB, and a subglacial erosion below current sea level reflects the intensive erosive power of Pleistocene glacial advances. Overdeepening in UEB and UB reaches 449 m depth (-53 m a.s.l.) and 216 m depth (180 m a.s.l.), respectively.

The extensive seismic data set allowed the identification of 23 fault planes in OB and UEB and five fault planes in UB. The 23 fault planes identified in the OB and UEB can be grouped into three fault clusters. The most northwestern cluster three in UEB agrees well with existing Mesozoic offshore and onshore faults. Cluster 2 overlaps with deep-seated faults mapped with previous offshore seismic data. These faults are apparently associated with major course changes of the central bedrock channel. Cluster 1 coincides with deep-seated offshore faults and lies in direct prolongation of various onshore fault systems (St. Gallen Fault Zone, Roggwil Fault Zone). Structures mapped in the bedrock underneath the UB connect well with onshore fault zones of the Hegau-Bodensee Graben. Quaternary graben structures suggest recent activity for some of these faults.

The multi-disciplinary approach, combining different multi-vintage seismic datasets with bathymetric data and a short-core transect also allowed to identify a very recently active fault structure offsetting the lake bottom (FID 6, Kippenhorn Fault). This structure, located within fault cluster 1, is associated with a mass-movement induced turbiditic event probably between CE 1895 and 1910/1911. It represents a NNW-SSE striking, ENE-dipping normal fault forming part of a negative flower structure rooted in the Miocene bedrock and is interpreted as a northward prolongation of the St. Gallen Fault Zone, located onshore ~ 10 km south of it. The present-day SHmax orientations of NNW-SSE promote reactivation of the SFZ and Kippenhorn Fault in sinistral strike-slip mode. The ~ 1 km long and 0.54 km² large Kippenhorn Fault qualifies for

minimum $M_W = 4.3\text{--}4.8$ earthquakes, when solely triggered without a connection to the SFZ. Several indications (fault orientation, alignment, SHmax direction) point towards a connection of the Kippenhorn Fault to the SFZ, supporting a significantly larger fault capable of causing much larger magnitudes ($M_W > 6$).

This study shows how the combination of various geophysical and geological datasets in perialpine lacustrine settings, with low crustal deformation rate, can help to identify potential seismogenic fault structures. Such field observations may be one additional tool to supplement the instrumental earthquake catalogues to better constrain seismic hazard assessments in the future.

DATA AVAILABILITY STATEMENT

The original contributions presented in the study are included in the article/**Supplementary Material**, further inquiries can be directed to the corresponding author.

AUTHOR CONTRIBUTIONS

SF, MW, HM, MH, RA, UW-S, and FA designed the study. SF, SK, KL, and MW acquired the multi-channel reflection seismic data. SF, MW, CA, FA acquired the 2019 seismic data and the short cores. CA and FA analyzed the short cores. SF and KL processed the seismic data. HP analyzed the offshore seismic data from the 1980s (Prakla Seismos GmbH, 1982) within the project ACoRE-B at the alpS GmbH (Centre for Climate Change Adaptation) and the Institute of Geology, University of Innsbruck. SF, SH, and HM created the figures and SF wrote the manuscript. HM and SH provided the tectonic profiles. All authors reviewed the manuscript.

REFERENCES

- Allen, P. A., Homewood, P., and Williams, G. D. (1986). Foreland Basins: An Introduction. *Foreland Basins* 8, 3–12. doi:10.1002/9781444303810.ch
- Beck, C., Reyss, J.-L., Leclerc, F., Moreno, E., Feuillet, N., Barrier, L., et al. (2012). Identification of Deep Subaqueous Co-seismic Scarps through Specific Coeval Sedimentation in Lesser Antilles: Implication for Seismic hazard. *Nat. Hazards Earth Syst. Sci.* 12 (5), 1755–1767. doi:10.5194/nhess-12-1755-2012
- Becker, A., Davenport, C. A., and Giardini, D. (2002). Palaeoseismicity Studies on End-Pleistocene and Holocene lake Deposits Around Basle, Switzerland. *Geophys. J. Int.* 149 (3), 659–678. doi:10.1046/j.1365-246x.2002.01678.x
- Bini, A., Buoncristiani, J.-F., Couterrand, S., Ellwanger, D., Felber, M., Florineth, D., et al. (2009). *Switzerland during the Last Glacial Maximum 1: 500'000*. Wabern bei Bern: Bundesamt für Landestopografie swisstopo.
- Bouroullac, R., Cartwright, J. A., Johnson, H. D., Lansigu, C., Quémerer, J.-M., and Savanier, D. (2004). Syndepositional Faulting in the Grès d'Annot Formation, SE France: High-Resolution Kinematic Analysis and Stratigraphic Response to Growth Faulting. *Geol. Soc. Lond. Spec. Publications* 221 (1), 241–265. doi:10.1144/gsl.sp.2004.221.01.13
- Brengman, C. M. J., Barnhart, W. D., Mankin, E. H., and Miller, C. N. (2019). Earthquake-Scaling Relationships from Geodetically Derived Slip Distributions. *Bull. Seismological Soc. America* 109 (5), 1701–1715. doi:10.1785/0120190048

FUNDING

This project was financially supported by the Swiss Commission for Geophysics (SGPK), Bundesamt für Landestopografie swisstopo, Nationale Genossenschaft für die Lagerung radioaktiver Abfälle Nagra, Landesanstalt für Umwelt Baden Württemberg, Landesamt für Geologie, Rohstoffe und Bergbau Baden Württemberg (LGRB).

ACKNOWLEDGMENTS

We thank the captains Andreas Schießl and Kurt Sarembe for maneuvering the Research vessel Kormoran, provided by Institut für Seenforschung ISF Langenargen. We are thankful for the technical help of Heiko Jähmlich, maintaining the seismic equipment. We appreciate the detailed comments and suggestions of Angela Landgraf, and Tobias Diehl, what improved the quality of the manuscript. The processing of the seismic reflection data was performed with SeisSpace/ProMAX provided through Halliburton/Landmark's University Grant Program and the stratigraphy was interpreted with Kingdom Suite 2015.0 provided by IHS. SRTM one Arc-Second data was provided by the United States Geological survey. The project ACoRE-B was funded by the Austrian Research Promotion Agency (FFG) and the Illwerke-Alternativenergie GmbH in the framework of the COMET program. We are thankful for the constructive comments of the two reviewers.

SUPPLEMENTARY MATERIAL

The Supplementary Material for this article can be found online at: <https://www.frontiersin.org/articles/10.3389/feart.2021.670532/full#supplementary-material>

- Buechi, M. W., Frank, S. M., Graf, H. R., Menzies, J., and Anselmetti, F. S. (2017). Subglacial Emplacement of Tills and Meltwater Deposits at the Base of Overdeepened Bedrock Troughs. *Sedimentology* 64 (3), 658–685. doi:10.1111/sed.12319
- Buechi, M. W., Graf, H. R., Haldimann, P., Lowick, S. E., and Anselmetti, F. S. (2018). Multiple Quaternary Erosion and Infill Cycles in Overdeepened Basins of the Northern Alpine Foreland. *Swiss J. Geosciences* 111 (1-2), 133–167. doi:10.1007/s00015-017-0289-9
- Cazzini, F. F., Amadori, C., Bosino, A., and Fantoni, R. (2020). New Seismic Evidence of the Messinian Paleomorphology beneath Lake Maggiore Area (Italy). *Jig* 139 (2), 195–211. doi:10.3301/jig.2019.26
- Chinnery, M. A. (1969). Earthquake Magnitude and Source Parameters. *Bull. Seismological Soc. America* 59 (5), 1969–1982. doi:10.1785/bssa0590051969
- Chopra, S., Castagna, J., and Portnaguine, O. (2006). Seismic Resolution and Thin-Bed Reflectivity Inversion. *CSEG recorder* 31 (1), 19–25. doi:10.1190/1.2369941
- Clark, P. U., Dyke, A. S., Shakun, J. D., Carlson, A. E., Clark, J., Wohlfarth, B., et al. (2009). The Last Glacial Maximum. *Science* 325 (5941), 710–714. doi:10.1126/science.1172873
- Dal Zilio, L., Kissling, E., Gerya, T., and van Dinther, Y. (2020). Slab Rollback Orogeny Model: A Test of Concept. *Geophys. Res. Lett.* 47 (18), e2020GL089917. doi:10.1029/2020gl089917
- de La Taille, C., Jouanne, F., Crouzet, C., Beck, C., Jomard, H., de Rycker, K., et al. (2015). Impact of Active Faulting on the post LGM Infill of Le Bourget Lake

- (Western Alps, France). *Tectonophysics* 664, 31–49. doi:10.1016/j.tecto.2015.08.024
- Diehl, T., Clinton, J., Cauzzi, C., Kraft, T., Kästli, P., Deichmann, N., et al. (2021). Earthquakes in Switzerland and Surrounding Regions during 2017 and 2018. *Swiss J. Geosciences* 114 (1), 4. doi:10.1186/s00015-020-00382-2
- Diehl, T., Kraft, T., Kissling, E., and Wiemer, S. (2017). The Induced Earthquake Sequence Related to the St. Gallen Deep Geothermal Project (Switzerland): Fault Reactivation and Fluid Interactions Imaged by Microseismicity. *J. Geophys. Res. Solid Earth* 122 (9), 7272–7290. doi:10.1002/2017jb014473
- Diehl, T., Madritsch, H., and Schnellmann, M. (2020). “Seismotectonic Evidence for Active Transtension along the Bodensee-Hegau Graben in the Low-Strain Region of the Northern Alpine Foreland,” in 18 th Swiss Geoscience Meeting, Zurich, 2020, 18, 1..
- Dürst Stucki, M., and Schlunegger, F. (2013). Identification of Erosional Mechanisms during Past Glaciations Based on a Bedrock Surface Model of the central European Alps. *Earth Planet. Sci. Lett.* 384 (-), 57–70. doi:10.1016/j.epsl.2013.10.009
- Egli, D., Mosar, J., Ibele, T., and Madritsch, H. (2016). The Role of Precursory Structures on Tertiary Deformation in the Black Forest—Hegau Region. *Int. J. Earth Sci.* 106, 2297–2318. doi:10.1007/s00531-016-1427-8
- Fabbri, S. C., Buechi, M. W., Horstmeyer, H., Hilbe, M., Hübscher, C., Schmelzbach, C., et al. (2018). A Subaquatic Moraine Complex in Overdeepened Lake Thun (Switzerland) Unravelling the Deglaciation History of the Aare Glacier. *Quat. Sci. Rev.* 187, 62–79. doi:10.1016/j.quascirev.2018.03.010
- Fabbri, S. C., Herwegh, M., Horstmeyer, H., Hilbe, M., Hübscher, C., Merz, K., et al. (2017). Combining Amphibious Geomorphology with Subsurface Geophysical and Geological Data: A Neotectonic Study at the Front of the Alps (Bernese Alps, Switzerland). *Quat. Int.* 451, 101–113. doi:10.1016/j.quaint.2017.01.033
- Fäh, D., Giardini, D., Kästli, P., Deichmann, N., Gisler, M., Schwarz-Zanetti, G., et al. (2011). *ECOS-09 Earthquake Catalogue of Switzerland Release 2011 Report and databasePublic Catalogue*, 17. 4. 2011. *Swiss Seismological Service ETH Zurich: Report SED/RISK*.
- Finckh, P. G. (1978). Are Southern Alpine Lakes Former Messinian Canyons? - Geophysical Evidence for Preglacial Erosion in the Southern Alpine Lakes. *Mar. Geology* 27 (3), 289–302. doi:10.1016/0025-3227(78)90036-1
- Finckh, P., Kelts, K., and Lambert, A. (1984). Seismic Stratigraphy and Bedrock Forms in Perialpine Lakes. *Geol. Soc. America Bull.* 95 (9), 1118–1128. doi:10.1130/0016-7606(1984)95<1118:ssabfi>2.0.co;2
- Gasperini, L., Marzocchi, A., Mazza, S., Miele, R., Meli, M., Najjar, H., et al. (2020). Morphotectonics and Late Quaternary Seismic Stratigraphy of Lake Garda (Northern Italy). *Geomorphology* 371, 107427. doi:10.1016/j.geomorph.2020.107427
- Gastineau, R., de Sigoyer, J., Sabatier, P., Fabbri, S. C., Anselmetti, F. S., Develle, A. L., et al. (2021). Active Subaquatic Fault Segments in Lake Iznik along the Middle Strand of the North Anatolian Fault, NW Turkey. *Tectonics* 40 (1), e2020TC006404. doi:10.1029/2020tc006404
- Gilli, A., Anselmetti, F. S., Ariztegui, D., and McKenzie, J. A. (2003). “A 600-year Sedimentary Record of Flood Events from Two Sub-alpine Lakes (Schwendiseen, Northeastern Switzerland),” in *Lake Systems from the Ice Age to Industrial Time*. Basel: Springer, 49–58. doi:10.1007/978-3-0348-7992-7_7
- Gilli, A., Anselmetti, F. S., Glur, L., and Wirth, S. B. (2013). “Lake Sediments as Archives of Recurrence Rates and Intensities of Past Flood Events,” in *Dating Torrential Processes on Fans and Cones: Methods and Their Application for Hazard and Risk Assessment*. Dordrecht: Dordrecht, 225–242. doi:10.1007/978-94-007-4336-6_15
- Goldfinger, C., Nelson, C. H., Morey, A. E., Johnson, J. E., Patton, J. R., Karabanov, E. B., et al. (2012). *Turbidite Event History—Methods and Implications for Holocene Paleoseismicity of the Cascadia Subduction Zone*. Reston: U.S. Geological Survey, 1661F.
- Goldfinger, C. (2011). Submarine Paleoseismology Based on Turbidite Records. *Annu. Rev. Mar. Sci.* 3 (1), 35–66. doi:10.1146/annurev-marine-120709-142852
- Hansch, S., Wessels, M., Niessen, F., and Schwab, A. (2009). Late Quaternary lake Response to Climate Change and Anthropogenic Impact: Biomarker Evidence from Lake Constance Sediments. *J. Paleolimnol.* 41 (3), 393–406. doi:10.1007/s10933-008-9232-4
- Harms, U., Raschke, U., Anselmetti, F. S., Strasser, M., Wittig, V., Wessels, M., et al. (2020). Hipercoring - an Innovative Hydraulic Coring System Recovering over 60 M Long Sediment Cores from Deep Perialpine Lakes. *Sci. Dril.* 28, 29–41. doi:10.5194/sd-28-29-2020
- Heidbach, O., Rajabi, M., Cui, X., Fuchs, K., Müller, B., Reinecker, J., et al. (2018). The World Stress Map Database Release 2016: Crustal Stress Pattern across Scales. *Tectonophysics* 744, 484–498. doi:10.1016/j.tecto.2018.07.007
- Heidbach, O., and Reinecker, J. (2013). *Analyse des rezenten Spannungsfelds der Nordschweiz*. Wettingen, Switzerland: NAGRA NAB12-05), p. 146.
- Heuberger, S., Roth, P., Zingg, O., Naef, H., and Meier, B. P. (2016). The St. Gallen Fault Zone: a Long-Lived, Multiphase Structure in the North Alpine Foreland Basin Revealed by 3D Seismic Data. *Swiss J. Geosci.* 109 (1), 83–102. doi:10.1007/s00015-016-0208-5
- Hofmann, F., Schlatter, R., and Weh, M., (2000). *Blatt 1011 Beggingen (Südhälfte) mit SW-Anteil von Blatt 1012 Singen*. (Swisstopo, Wabern), p. p. 113.
- Houlié, N., Woessner, J., Giardini, D., and Rothacher, M. (2018). Lithosphere Strain Rate and Stress Field Orientations Near the Alpine Arc in Switzerland. *Scientific Rep.* 8 (1), 2018. doi:10.1038/s41598-018-20253-z
- Huber, M. L., Amschwand, D., Madritsch, H., Deplazes, G., and Buechi, M. W. (2020). *Quaternary Borehole QBO Trüllikon-Rudolfingen (QTRU) - Data Report*. Wettingen, Switzerland: Nagra, 18.
- Hughes, P. D., Gibbard, P. L., and Ehlers, J. (2013). Timing of Glaciation during the Last Glacial Cycle: Evaluating the Concept of a Global ‘Last Glacial Maximum’ (LGM). *Earth-Science Rev.* 125, 171–198. doi:10.1016/j.earscirev.2013.07.003
- Ibele, T., (2015). Tectonics of the Hegau and Lake Constance Region: a Synthesis Based on Existing Literature. Nagra working report, NAB 12-23), p. 70.
- Kastrup, U., Zoback, M. L., Deichmann, N., Evans, K. F., Giardini, D., and Michael, A. J. (2004). Stress Field Variations in the Swiss Alps and the Northern Alpine Foreland Derived from Inversion of Fault Plane Solutions. *J. Geophys. Research-Solid Earth* 109 (B01402), 1–22. doi:10.1029/2003jb002550
- Kremer, K., Corella, J. P., Adatte, T., Garnier, E., Zenhäusern, g., and Girardclos, S. (2015a). Origin of Turbidites in Deep Lake Geneva (France-Switzerland) in the Last 1500 Years. *J. Sediment. Res.* 85 (12), 1455–1465. doi:10.2110/jsr.2015.92
- Kremer, K., Gassner-Stamm, G., Grolimund, R., Wirth, S. B., Strasser, M., and Fäh, D. (2020). A Database of Potential Paleoseismic Evidence in Switzerland. *J. Seismol.* 24 (2), 247–262. doi:10.1007/s10950-020-09908-5
- Kremer, K., Hilbe, M., Simpson, G., Decrouy, L., Wildi, W., and Girardclos, S. (2015b). Reconstructing 4000 Years of Mass Movement and Tsunami History in a Deep Peri-Alpine lake (Lake Geneva, France-Switzerland). *Sedimentology* 62 (5), 1305–1327. doi:10.1111/sed.12190
- Lemke, D. (2018). *Seismic Facies Analysis of Lake Überlingen by Means of High-Resolution 2D Seismics*. Germany: Faculty of Mathematics and Natural Sciences, University of Kiel. Bachelor Thesis.
- LUBW (2011). *Langzeitverhalten der Bodensee-Wasserstände*. Karlsruhe: UBW Landesanstalt für Umwelt, Messungen und Naturschutz Baden-Württemberg, 234.
- Madritsch, H., Naef, H., Meier, B., Franzke, H. J., and Schreurs, G. (2018). Architecture and Kinematics of the Constance-Frick Trough (Northern Switzerland): Implications for the Formation of Post-Variscan Basins in the Foreland of the Alps and Scenarios of Their Neogene Reactivation. *Tectonics* 37 (7), 2197–2220. doi:10.1029/2017tc004945
- Madritsch, H., Preusser, F., Fabbri, O., Bichet, V., Schlunegger, F., and Schmid, S. M. (2010). Late Quaternary Folding in the Jura Mountains: Evidence from Syn-Erosional Deformation of Fluvial Meanders. *Terra Nova* 22 (2), 147–154. doi:10.1111/j.1365-3121.2010.00928.x
- Magrani, F., Valla, P. G., Gribenski, N., and Serra, E. (2020). Glacial Overdeepenings in the Swiss Alps and Foreland: Spatial Distribution and Morphometrics. *Quat. Sci. Rev.* 243, 106483. doi:10.1016/j.quascirev.2020.106483
- Malz, A., Madritsch, H., Meier, B., and Kley, J. (2016). An Unusual triangle Zone in the External Northern Alpine Foreland (Switzerland): Structural Inheritance, Kinematics and Implications for the Development of the Adjacent Jura Fold-And-Thrust belt. *Tectonophysics* 670, 127–143. doi:10.1016/j.tecto.2015.12.025
- McCalpin, J. P., and Nelson, A. R. (2009). “Chapter 1 Introduction to Paleoseismology,” in *Paleoseismology*. 2nd Edition, 95. London: Elsevier, 1–27. doi:10.1016/s0074-6142(09)95001-x
- McHugh, C. M. G., Braudy, N., Çağatay, M. N., Sorlien, C., Cormier, M.-H., Seeber, L., et al. (2014). Seafloor Fault Ruptures along the North Anatolia Fault in the Marmara Sea, Turkey: Link with the Adjacent basin Turbidite Record. *Mar. Geology* 353, 65–83. doi:10.1016/j.margeo.2014.03.005

- Meghraoui, M., Delouis, B., Ferry, M., Giardini, D., Huggenberger, P., Spottke, I., et al. (2001). Active normal Faulting in the Upper Rhine Graben and Paleoseismic Identification of the 1356 Basel Earthquake. *Science* 293 (5540), 2070–2073. doi:10.1126/science.1010618
- Mey, J., Scherler, D., Wickert, A. D., Egholm, D. L., Tesauero, M., Schildgen, T. F., et al. (2016). *Glacial Isostatic Uplift of the European Alps*. London: Nature Communications, 7, 13382. doi:10.1038/ncomms13382
- Michetti, A. M., Audemard, F. A., and Marco, S. (2005). Future Trends in Paleoseismology: Integrated Study of the Seismic Landscape as a Vital Tool in Seismic hazard Analyses. *Tectonophysics* 408 (1-4), 3–21. doi:10.1016/j.tecto.2005.05.035
- Mix, A., Bard, E., and Schneider, R. (2001). Environmental Processes of the Ice Age: Land, Oceans, Glaciers (EPILOG). *Quat. Sci. Rev.* 20 (4), 627–657. doi:10.1016/s0277-3791(00)00145-1
- Mock, S., and Herwegh, M. (2017). Tectonics of the central Swiss Molasse Basin: Post-Miocene Transition to Incipient Thick-Skinned Tectonics?. *Tectonics* 36 (9), 1699–1723. doi:10.1002/2017tc004584
- Moernaut, J., Daele, M. V., Heirman, K., Fontijn, K., Strasser, M., Pino, M., et al. (2014). Lacustrine Turbidites as a Tool for Quantitative Earthquake Reconstruction: New Evidence for a Variable Rupture Mode in South central Chile. *J. Geophys. Res. Solid Earth* 119 (3), 1607–1633. doi:10.1002/2013jb010738
- Monecke, K., Anselmetti, F. S., Becker, A., Sturm, M., and Giardini, D. (2004). The Record of Historic Earthquakes in lake Sediments of Central Switzerland. *Tectonophysics* 394 (1-2), 21–40. doi:10.1016/j.tecto.2004.07.053
- Monegato, G., Ravazzi, C., Donegana, M., Pini, R., Calderoni, G., and Wick, L. (2007). Evidence of a Two-fold Glacial advance during the Last Glacial Maximum in the Tagliamento End Moraine System (Eastern Alps). *Quat. Res.* 68 (2), 284–302. doi:10.1016/j.yqres.2007.07.002
- Müller, G., and Gees, R. A. (1968). Origin of the Lake Constance Basin. *Nature* 217 (5131), 836–837. doi:10.1038/217836a0
- Naef, H., Birkhäuser, P., and Roth, P. (1995). *Interpretation der Reflexionsseismik im Gebiet nördlich Lägeren - Zürcher Weinland*. Nagra-Technical Report - NTB94-14. Wettingen: Nagra.
- Niessen, F., Sturm, M., Schröder, H. G., Giovanoli, F., and Ostendorf, W. (1990). Beiträge zur Landschafts- und Siedlungsgeschichte am Bodensee-Untersee: paläolimnologische Untersuchungen. *Bericht der Römisch-Germanischen Kommission* 71 (1), 245–308.
- Ortner, H., Aichholzer, S., Zerlauth, M., Pilsner, R., and Fügenschuh, B. (2015). Geometry, Amount, and Sequence of Thrusting in the Subalpine Molasse of Western Austria and Southern Germany, European Alps. *Tectonics* 34 (1), 1–30. doi:10.1002/2014tc003550
- Oswald, P., Moernaut, J., Fabbri, S., De Batist, M., Hajdas, I., Ortner, H., et al. (2021). Combined On-Fault and Off-Fault Paleoseismic Evidence in the Postglacial Infill of the Inner-Alpine Lake Achensee (Austria, Eastern Alps). *Front. Earth Sci.* 9. doi:10.3389/feart.2021.670952
- Pfiffner, O. (1986). Evolution of the North Alpine Foreland Basin in the central Alps. *Foreland basins* 8, 219–228.
- Pomella, H., Ortner, H., Zerlauth, M., and Fügenschuh, B. (2015). The Alpine Nappe Stack in Western Austria: a Crustal-Scale Cross Section. *Int. J. Earth Sci. (Geol Rundsch)* 104 (3), 733–745. doi:10.1007/s00531-014-1097-3
- Prakla Seismos GmbH (1982). *Bericht über reflexionsseismische Messungen am Bodensee 1980/81*. Prakla seismos.
- Preusser, F., Reitner, J. M., and Schlüchter, C. (2010). Distribution, Geometry, Age and Origin of Overdeepened Valleys and Basins in the Alps and Their Foreland. *Swiss J. Geosci.* 103 (3), 407–426. doi:10.1007/s00015-010-0044-y
- Reber, R., and Schlunegger, F. (2016). Unravelling the Moisture Sources of the Alpine Glaciers Using Tunnel Valleys as Constraints. *Terra Nova* 28 (3), 202–211. doi:10.1111/ter.12211
- Ring, U., and Gerdes, A. (2016). Kinematics of the Alpenrhein-Bodensee Graben System in the Central Alps: Oligocene/Miocene Transtension Due to Formation of the Western Alps Arc. *Tectonics* 35 (6), 1367–1391. doi:10.1002/2015tc004085
- Ritz, J.-F., Baize, S., Ferry, M., Larroque, C., Audin, L., Delouis, B., et al. (2020). Surface Rupture and Shallow Fault Reactivation during the 2019 Mw 4.9 Le Teil Earthquake, France. *Commun. Earth Environ.* 1 (1), 10. doi:10.1038/s43247-020-0012-z
- Rodriguez-Pascua, M. A., Calvo, J. P., De Vicente, G., and Gomez-Gras, D. (2000). Soft-sediment Deformation Structures Interpreted as Seismites in Lacustrine Sediments of the Prebetic Zone, SE Spain, and Their Potential Use as Indicators of Earthquake Magnitudes during the Late Miocene. *Sediment. Geology*. 135 (1-4), 117–135.
- Roth, P., Naef, H., and Schnellmann, M. (2010). *Kompilation und Interpretation der Reflexionsseismik im Tafeljura und Molassebecken der Zentral- und Nordostschweiz*. Wettingen: Nagra Arbeitsbericht NAB 10-39.
- Sammartini, M., Moernaut, J., Kopf, A., Stegmann, S., Fabbri, S. C., Anselmetti, F. S., et al. (2021). Propagation of Frontally Confined Subaqueous Landslides: Insights from Combining Geophysical, Sedimentological, and Geotechnical Analysis. *Sediment. Geology*. 416, 105877. doi:10.1016/j.sedgeo.2021.105877
- Schlunegger, F., and Kissling, E. (2015). Slab Rollback Orogeny in the Alps and Evolution of the Swiss Molasse basin. *Nat. Commun.* 6. doi:10.1038/ncomms9605
- Schnellmann, M., Anselmetti, F. S., Giardini, D., and McKenzie, J. A. (2006). 15,000 Years of Mass-Movement History in Lake Lucerne: Implications for Seismic and Tsunami Hazards. *Eclogae Geol. Helv.* 99 (3), 409–428. doi:10.1007/s00015-006-1196-7
- Schnellmann, M., Anselmetti, F. S., Giardini, D., McKenzie, J. A., and Ward, S. N. (2002). Prehistoric Earthquake History Revealed by Lacustrine Slump Deposits. *Geol* 30 (12), 1131–1134. doi:10.1130/0091-7613(2002)030<1131:pehrbl>2.0.co;2
- Schreiner, A. (1992). Hegau und westlicher Bodensee. *Geologische Karte von Baden-Württemberg 1:50 000, Erläuterungen*. Freiburg i. Br., Stuttgart: Geologisches Landesamt Baden-Württemberg, 290.
- Schwalb, A., Dean, W., Güde, H., Hanisch, S., Sobek, S., and Wessels, M. (2013). Benthic Ostracode $\delta^{13}C$ as Sensor for Early Holocene Establishment of Modern Circulation Patterns in Central Europe. *Quat. Sci. Rev.* 66, 112–122. doi:10.1016/j.quascirev.2012.10.032
- Schwestermann, T. (2016). *Mass-movement Event Stratigraphy in Lake Constance*. MSc Thesis, ETH Zurich, p. pp 90.
- Sommaruga, A., Eichenberger, U., and Marillier, F. (2012). “Seismic Atlas of the Swiss Molasse Basin,” in *Matér. Géol. Suisse – Géophysique*, 44, 88.
- Stirling, M., Rhoades, D., and Berryman, K. (2002). Comparison of Earthquake Scaling Relations Derived from Data of the Instrumental and Preinstrumental Era. *Bull. Seismological Soc. America* 92 (2), 812–830. doi:10.1785/0120000221
- Strasser, M., Monecke, K., Schnellmann, M., and Anselmetti, F. S. (2013). Lake Sediments as Natural Seismographs: A Compiled Record of Late Quaternary Earthquakes in Central Switzerland and its Implication for Alpine Deformation. *Sedimentology* 60 (1), 319–341. doi:10.1111/sed.12003
- Sturm, M., and Matter, A. (1978). Turbidites and Varves in Lake Brienz (Switzerland): Deposition of Clastic Detritus by Density Currents. *Spec. Publ. Int. Assoc. Sediment.* 2, 147–168. doi:10.1002/9781444303698.ch8
- Swisspetrol (1962). “Seismische Bohrlochmessungen in der Tiefbohrung Kreuzlingen 1, 1km WNW Dippishausen,” in *Swisspetrol Holding AG*, (Prakla Seismos GmbH).
- swisstopo (2005a). *Geologische Karte der Schweiz 1:500,000*. Wabern: Federal Office of Topography Swisstopo.
- swisstopo (2017). “Geologische Vektordatensätze GeoCover,” in *Wabern: Federal Office of Topography Swisstopo*.
- swisstopo (2005b). *Tektonische Karte der Schweiz 1:500,000*. Wabern: Federal Office of Topography Swisstopo.
- Ustaszewski, M. E., Hampel, A., and Pfiffner, O. A. (2008). Composite Faults in the Swiss Alps Formed by the Interplay of Tectonics, Gravitation and Postglacial Rebound: an Integrated Field and Modelling Study. *Swiss J. Geosci.* 101 (1), 223–235. doi:10.1007/s00015-008-1249-1
- Ustaszewski, M., Herwegh, M., McClymont, A. F., Pfiffner, O. A., Pickering, R., and Preusser, F. (2007). Unravelling the Evolution of an Alpine to post-glacially Active Fault in the Swiss Alps. *J. Struct. Geology*. 29 (12), 1943–1959. doi:10.1016/j.jsg.2007.09.006
- van Rensbergen, P., de Batist, M., Beck, C., and Chapron, E. (1999). High-resolution Seismic Stratigraphy of Glacial to Interglacial Fill of a Deep Glacigenic lake: Lake Le Bourget, Northwestern Alps, France. *Sediment. Geology*. 128 (1), 99–129. doi:10.1016/s0037-0738(99)00064-0
- Van Rensbergen, P., De Batist, M., Beck, C., and Manalt, F. (1998). High-resolution Seismic Stratigraphy of Late Quaternary Fill of Lake Annecy (Northwestern

- Alps): Evolution from Glacial to Interglacial Sedimentary Processes. *Sediment. Geology*. 117 (1), 71–96. doi:10.1016/s0037-0738(97)00123-1
- Wells, D. L., and Coppersmith, K. J. (1994). New Empirical Relationships Among Magnitude, Rupture Length, Rupture Width, Rupture Area, and Surface Displacement. *Bull. Seismological Soc. America* 84 (4), 974–1002
- Wessels, M., Anselmetti, F., Artuso, R., Baran, R., Daut, G., Gaide, S., et al. (2015). Bathymetry of Lake Constance – a High-Resolution Survey in a Large, Deep Lake. *ZfV - Z. Geodäsie, Geoinformation Landmanagement* 140 (4/2015), 203. doi:10.12902/zfv-0079-2015
- Wessels, M., Bussmann, I., Schloemer, S., ter, M. S., and dere, V. B. (2010). Distribution, Morphology, and Formation of Pockmarks in Lake Constance, Germany. *Limnol. Oceanogr.* 55 (6), 2623–2633. doi:10.4319/lo.2010.55.6.2623
- Wessels, M., Mohaupt, K., Kümmerlin, R., and Lenhard, A. (1999). Reconstructing Past Eutrophication Trends from Diatoms and Biogenic Silica in the Sediment and the Pelagic Zone of Lake Constance, Germany. *J. Paleolimnology* 21 (2), 171–192. doi:10.1023/a:1008080922586
- Wessels, M. (1998). Natural Environmental Changes Indicated by Late Glacial and Holocene Sediments from Lake Constance, Germany. *Palaeogeogr. Palaeoclimatol. Palaeoecol.* 140 (1-4), 421–432. doi:10.1016/s0031-0182(98)00026-1
- Wessels, M. (2003). *Sedimente im Bodensee - Bestandsaufnahme 2003*. doi:10.1515/9783110898774
- Widess, M. B. (1973). How Thin Is a Thin Bed?. *Geophysics* 38 (6), 1176–1180. doi:10.1190/1.1440403
- Wiemer, S., Giardini, D., Fäh, D., Deichmann, N., and Sellami, S. (2009). Probabilistic Seismic hazard Assessment of Switzerland: Best Estimates and Uncertainties. *J. Seismol* 13 (4), 449–478. doi:10.1007/s10950-008-9138-7
- Winterberg, S., Picotti, V., and Willett, S. D. (2020). Messinian or Pleistocene valley Incision within the Southern Alps. *Swiss J. Geosciences* 113 (1), 7. doi:10.1186/s00015-020-00361-7
- Wong, G. S. K., and Zhu, S. M. (1995). Speed of Sound in Seawater as a Function of Salinity, Temperature, and Pressure. *The J. Acoust. Soc. America* 97 (3), 1732–1736. doi:10.1121/1.413048
- Wood, R. M. (1989). “Extraordinary Deglaciation Reverse Faulting in Northern Fennoscandia,” in *Earthquakes at North-Atlantic Passive Margins: Neotectonics and Postglacial Rebound*. Dordrecht: Springer, 141–173. doi:10.1007/978-94-009-2311-9_10
- Zerlauth, M., Ortner, H., Pomella, H., Adrian Pfiffner, O., and Fügenschuh, B. (2014). Inherited Tectonic Structures Controlling the Deformation Style: an Example from the Helvetic Nappes of the Eastern Alps. *Swiss J. Geosci.* 107 (2), 157–175. doi:10.1007/s00015-014-0167-7

Conflict of Interest: The authors declare that the research was conducted in the absence of any commercial or financial relationships that could be construed as a potential conflict of interest.

Publisher’s Note: All claims expressed in this article are solely those of the authors and do not necessarily represent those of their affiliated organizations, or those of the publisher, the editors and the reviewers. Any product that may be evaluated in this article, or claim that may be made by its manufacturer, is not guaranteed or endorsed by the publisher.

Copyright © 2021 Fabbri, Affentranger, Krastel, Lindhorst, Wessels, Madritsch, Allenbach, Herwegh, Heuberger, Wielandt-Schuster, Pomella, Schwestermann and Anselmetti. This is an open-access article distributed under the terms of the Creative Commons Attribution License (CC BY). The use, distribution or reproduction in other forums is permitted, provided the original author(s) and the copyright owner(s) are credited and that the original publication in this journal is cited, in accordance with accepted academic practice. No use, distribution or reproduction is permitted which does not comply with these terms.